Longitudinal features of day- and night-time ionospheric annual variations during the solar cycles 23 and 24

Waqar Younas, Majid Khan, C. Amory-Mazaudier

Longitudinal Features of Day- and Night-time Ionospheric Annual Variations During the Solar Cycles 23 and 24.

Waqar Younas[1], Majid Khan[1] and C. Amory-Mazudier [2]

[1]Department of Physics, Quaid-i-Azam University Islamabad 45320, Pakistan

[2]Sorbonne Université, Ecole polytechnique, Institut Polytechnique de Paris, Université Paris Saclay, Observatoire de Paris, CNRS, Laboratoire de Physique des Plasmas (LPP), 75005 Paris, France

Corresponding author: Dr. Majid Khan (majid.khan@qau.edu.pk)

Key Words

Abstract

We present a study concerning the ionospheric annual variations (IAV) using the global ionospheric maps (GIMs). In this regard, the corresponding regional electron content (REC) is computed in four longitudinal sectors, namely Asia, Africa, America and Pacific. The features of day- and night-time IAV are investigated using (i) band-pass filters and (ii) summer to winter (SW) ratio of REC. The results indicate that IAV are stronger in the southern hemisphere as compared to its northern counterpart. The asymmetry in the amplitude of IAV is maximum for the Pacific region, followed by America, Africa and Asia. The IAV in southern hemisphere are regular ionospheric variations (RIAV) with positive and negative peaks occurring in the months of December and June, respectively. The northern hemisphere and latitudinal regions exhibit a day-time anomalous ionospheric annual variations (AIAV), during the peak years of the considered solar cycles, in which maxima (minima) occurs in local winter (summer). In this regard, the phase of AIAV is found to vary with solar activity. The night-time IAV show anomalous behavior in the northern hemisphere during the solar minimum. The SW ratio of day-time REC is less than unity at northern hemisphere during the peak of a solar cycle. However, the said ratio is always greater than one in southern counterpart. The fitting curve for day-time SW ratio has a strong negative slope in the northern hemisphere and winter anomaly can be observed when sunspot number (SSN)>120. On the other hand, the correlation and fitting analysis demonstrate that night-time SW ratio enhances with increase in the solar activity. This result predicts that night- time winter anomaly can only be present during the periods of minimum and low solar activity.

1. Introduction

The terrestrial ionosphere is a dynamical region, which is subjected to several variations ranging from a few hours to several solar cycles (SCs). In this regard, ionospheric annual variation (IAV) refers to narrowband variation (or oscillation) with a period of one year and is identified by narrowband filtering of the regional electron content (REC) variations. The IAV is said to be a regular ionospheric annual variation (RIAV) if its maxima occur in the local summer whereas minima are found to be in the local winter. On the other hand, if maxima (minima) of IAV appears in the local winter (summer), it is termed as an anomalous ionospheric annual variation (AIAV) (Torr & Torr, 1973).

The mechanism responsible for the AIAV is not well understood and poses one of the major challenges to the ionospheric community (Rishbeth, 2007), usually the AIAV is explained with help of thermospheric O/N_2 variations, which are found to be greater in the local winter. This trend can be associated with the global circulation of thermospheric winds which up-well (down-well) O/N_2 rich air in summer (winter) hemisphere (Rishbeth, 1998; Zou et al., 2000; Yasyukevich et al., 2018). Recent studies have expanded the knowledge of AIAV using different observations and, ever improving, modelling techniques. Azpilicueta and Nava (2020) provided a different view of AIAV using the total electron content (TEC) data over an extended period (about two solar cycles) and demonstrated that the occurrence of AIAV depends on the geomagnetic latitudes.

Apart from the day-time AIAV, the night-time ionospheric AIAV is also observed in the several regions (Jakowski et al., 1990, Karia et al., 2019). Likewise, Jakowski et al. (2015) provided a confirmation of the night-time AIAV as observed in the northern hemisphere (American sectors) and in the southern part of the Asian longitudes during the low solar activities. Wang et al. (2021) studied the night-time AIAV by using the in-situ electron density measurements from the CSES (China Seismo-Electronmagnetic Satellite) orbiting above the F2 layer peak height (hmF2) region. Their results indicate that the night-time AIAV can appear at mid-latitudes of the American longitudes (northern winter time) and at the Asian longitudinal sectors (southern winter time), furthermore the said phenomenon can also appear in the equatorial regions.

Recently, Younas et al. (2023) studied the features of the IAV at low-, mid- and high-latitudes using the global ionospheric maps (GIMs); it indicates that the amplitude of IAV is greater in the southern hemisphere as compared to the northern counterpart. This asymmetry in the amplitude of IAV is maximum at low-latitude, followed by mid- and high-latitudes, respectively. They have also found that phase of annual variations at the respective latitudes varies with the SC.

The present work is an extension of Younas et al. (2023) with specific focus on longitudinal variability of the IAV; which allows us to investigate the day- and night-time IAV and to identify the regions of

AIAV. Here, we also highlight the variability of the IAV at low and low-latitudes of the considered longitudinal sectors.

The rest of manuscript is organized as follows: section 2 provides a detail about the ionospheric data sets and processing techniques used for the computation of IAV. The result and discussion are presented in section 3, whereas section 4 concludes the main finding of the study.

2. Data sets and data processing

We have used the UPC-UQRG maps (Béniguel et al., 2017) for the calculation of regional electron content (REC) in four longitudinal sectors, namely Asia, Africa, America and Pacific at low-, mid- and high-latitudes. Detailed information about the latitudinal and longitudinal limits of different regions, used in this work, is depicted in table 1. The REC is computed by multiplying the vertical total electron content (vTEC) of each GIM cell $I_{p,q}$ with corresponding area $A_{p,q}$ and then summing over the entire region (Younas et al., 2023; Afraimovich et al., 2006; Ratovsky et al., 2020), i.e.,

$$REC = \sum_{p,q} I_{p,q} A_{p,q} \qquad (1)$$

Here the indices p and q denote, respectively, the latitude and longitude of a particular GIM cell. The monthly averaged REC is evaluated by using five geomagnetically quiet days (https://wdc.kugi.kyoto-u.ac.jp/qddays/) of each month from 1999 to 2020.

The day- (and night-) time ionospheric REC is computed from the maximum (minimum) values of monthly averaged REC data, respectively. As we have considered only the REC, for which the effects associated with localized anomalies (Weddell Sea Anomaly and summer evening anomaly) may be ignored. For estimating the amplitude of IAV (day- and night-time) we have employed the band pass filters having a lower and upper bound of 11 and 13 months, respectively. Furthermore, the REC ratio of SW is evaluated by taking arithmetic ratio of June to January (January to June) in the northern (southern) hemisphere. Moreover, linear fitting and Pearson correlation (Benesty et al., 2009) is evaluated for both day- and night-time SW ratio. Table 2 highlights the main characteristics of SC-23 and 24.

3. Results

3.1 The IAV at four hemispheric longitudinal regions

Figure 1a (from top to 4th panel) presents the day-time IAV in hemispheric longitudinal sectors of Asia, Africa, America and Pacific from 1999 to 2020. On each panel, the northern and southern regions are presented by red and blue lines, respectively. While the 5th panel in same figure depicts the solar activity indices (SSN in blue and F10.7 in red). The southern hemisphere shows that all

four longitudinal sectors exhibit maxima and minima, orderly during the months of December and June, i.e., RIAV for the considered time period. Furthermore, the corresponding amplitude varies linearly with the solar activity. The maximum amplitude of RIAV in the southern hemisphere occurs in the Pacific region (0.1589GECU in Dec. 2002), followed by America (0.1334GECU), Africa (0.0976GECU) and Asia (0.0598GECU).

On the other hand, the phase of the IAV in the northern hemisphere changes with the solar activity in all of the considered regions. During the high solar activity and descending phase of SC- 23, i.e., 2000-2005, we can observe that the IAV in the northern hemisphere becomes in-phase with the southern counterpart. Hence, during these years, maxima (minima) occurs in December (June), which corresponds to the AIAV. Whereas, as the solar activity weakens, the peak of IAV in the northern hemisphere shifts to June, and during the solar minimum the amplitude of IAV becomes negligibly small.

Figure 1b is similar to Fig. 1a but for the night-time IAV, which are found to be completely out of phase in both hemispheres during the rising and declining phase of solar cycle. The maxima (minima) occurs in the month of June (December) and December (June), respectively in the northern and southern hemispheres, i.e., these are RIAV. However, amplitude of IAV in the northern parts of Africa and America region become almost zero during the years of deep solar minimum 2006-2009. Moreover, the amplitude of night-time IAV varies with the solar activity and exhibits a hemispheric asymmetry in the amplitude for the said variations. In particular, the northern hemisphere is found to have low amplitude as compared to its southern counterpart in all of the considered regions. This asymmetry – in the amplitude of night-time IAV – is found to be maximum for Africa, followed by America, Pacific and Asia, respectively. During the deep solar minimum, i.e., from 2006 to 2009, the IAV becomes almost zero in the northern hemisphere.

Figure 2a (top), presents the ratio of SW day-time REC, in the northern hemisphere whereas middle panel shows the same ratio for the southern counterpart. The 3rd panel depicts the ratio of summer of southern to the winter of northern hemisphere. On each panel, Asia, Africa, America and Pacific regions are represented by blue, red, yellow and violet bars, respectively. Here we note that for the northern hemisphere SW ratio is less than unity for the years 1999-2002, 2010-2011, 2013-2014 and 2020. This corresponds to the fact that during these years the winter season has higher electron content than summer, called the winter anomaly (Rishbeth & Müller-Wodarg, 2006). Moreover, all of the considered sectors behave identically in the northern hemisphere. The ratio is minimum during the year 2001 when it reaches to 0.69 (Pacific region). The SW ratio in the southern hemisphere is much higher than unity for all the years. The Africa region exhibits a higher ratio than

other sectors during the considered period. This ratio is found to be maximum in the year 2011 and reaches up to a value of 3.14 (Africa). The summer (south) to winter (north) ratio of REC is found to be greater than unity for most of the years, we also note that the American sector depicts higher ratio than other regions. During the years 2000 and 2001, the said ratio drops to less than unity in all sectors except for American region.

Figure 2b is similar to Fig. 2a but for the night-time REC data. The night-time SW ratio (northern hemisphere) is found to be greater than unity for most of the considered years except for 2010, 2019 and 2020 (Africa and America regions only). The Pacific region is found to have higher SW ratio in the northern hemisphere for all the years. The night-time SW ratio of the southern hemisphere is much greater than unity, exhibiting a maximum value in the year 2001, followed by 2011 and 2020, respectively. The night-time summer (south) to winter (ratio) is also greater than 1, for all the years as depicted in Fig. 2b (bottom panel). The said ratio is minimum in 2009 where it reaches to a value of 1.2 (Asia region).

3.2 The IAV at four low-latitudes longitudinal regions

Figure 3a presents the day-time IAV at four low-latitudes longitudinal sectors, i.e., in Asia low-latitudes (ASLL), Africa low-latitudes (AFLL), America low-latitudes (AMLL) and Pacific low-latitudes (PALL) from 1999 to 2020. On each panel, the northern and southern hemispheric parts, of corresponding regions, are represented by red and blue lines, respectively. Here we note that the day-time annual oscillations in the southern low latitudinal regions exhibit maxima and minima in December and January, orderly. This corresponds to the RIAV in the southern hemisphere. The intensity of RIAV in the southern low-latitudes varies with the SC. Moreover, the RIAV in the southern low-latitude region manifest a maximum amplitude in PALL, followed, respectively by AMLL, AFLL and ASLL. On the other hand, the northern low-latitudes depict that variations in the day-time IAV amplitude correlate with the SC variations. The maxima (minima) of the said IAV in the northern hemisphere – during years of high solar activity – occurs during December (June) and it corresponds to AIAV. Whereas, these peak gradually shift with declining phase of the SC and reached in the month of May (November) in the years of solar minimum and ascending phase of SC-24 (i.e., from 2007 to 2011). The hemispheric asymmetry in the amplitude of day-time IAV is maximum for PALL, followed by AFLL, AMLL and ASLL, respectively.

Figure 3b is similar to Fig. 3a but for night-time IAV. The night-time IAV in southern low-latitudes corresponds to RIAV and its amplitude increases linearly with the SC intensity. The said RIAV at southern low-latitudes exhibits high amplitude during the peak of SC-23 as compared to 24. The southern hemisphere exhibits a uniform trend regarding the night-time RIAV at all the considered

longitudes. On the other hand, the northern low-latitude region depicts a mixed trend in night-time IAV. The peak of said oscillation is observed in April (May), while minima is found to occur in October (November) at ASLL and AFLL (AMLL and PALL) regions during the rising and declining phase of SC. However, the IAV becomes negligible at northern ASLL, AFLL and AMLL during the years of deep solar minimum. The night-time IAV at northern low-latitude has smaller amplitude than southern counterpart at corresponding longitudinal sectors. The amplitude of night-time IAV in the northern hemisphere is found to be maximum for PALL, followed orderly by AMLL, ASLL and AFLL regions.

Figure 4a depicts, from the top to bottom, the REC ratio of day-time SW (northern low-latitudes), SW (southern low-latitude regions) and ratio of day-time summer (south) to winter (north) for the period 1999 to 2020. It can be seen that the SW ratio in the northern low-latitudes is less then unity for the years 1999-2002, 2010-2011, 2013-2014 and 2020. The said ratio is found to be minimum during the year 2011 where it exhibit the values 0.64, 0.66, 0.76 and 0.67, orderly at ASLL, AFLL, AMLL and PALL. Whereas, we observe that the same ratio for the southern counterpart is greater than unity for all the considered years and is maximum in 2011 and minimum during 2016. The summer (south) to winter (north) REC ratio, as shown in last panel of Fig. 4a, is less than 1 during 2000, 2001, 2002 and 2014 at ASLL and AFLL regions, while for PALL this trend is observed in 2020. Figure 4b is similar to 4a but for night-time REC data. The night-time ratio of SW in the northern hemisphere is less than 1 in the AFLL and AMLL during the years of minimum solar activity. On the other hand, the same ratio for the night-time southern counterpart is greater than unity for most of the considered years and follows the SC. However, at PALL we note that the said ratio is less than 1 during the years 2007 and 2018.

3.3 The IAV at four mid-latitudes longitudinal regions

The day-time IAV at four mid-latitudinal regions, namely ASML, AFML, AMML and PAML are presented in Fig. 5a. Several interesting results can be extracted from this figure; the amplitude of IAV at northern mid-latitudinal region is less than southern counterpart and this asymmetry is maximum for PAML, followed by AMML, AFML and ASML, respectively. The southern low-latitudes exhibit RIAV with maxima (minima) occurring in December (June) whereas the amplitude of these RIAV is maximum for AMML (0.061 GECU in Dec 2002), followed by PAML (0.052 GECU Dec 2002), AFML (0.032 GECU Dec 2002) and ASML (0.011 GECU Dec 2002), respectively. Moreover, amplitude of day-time RIAV variations – in the southern mid-latitude regions except Asia – follows the SC trend. On the other hand, the phase of day-time IAV at the northern mid-latitude varies with the solar activity. From 1999 to 2004, the ASML north shows AIAV, and it depicts RIAV from 2006 to 2018.

The AMML and PAML north exhibit the AIAV during the peak years of SC-23 and RIAV during the solar minimum years.

Figure 5b is a night-time counterpart of Fig. 5a. The night-time IAVs at four mid-latitudinal regions are found to be RIAV, i.e., maxima and minima occur in the respective summer and winter seasons, respectively. The southern hemisphere manifests a higher amplitude of IAV than its northern counterpart at AMML and PAML, respectively. Whereas, the AFML exhibits almost equal amplitude of IAV at both hemispheric regions. The ASML north has a higher intensity of night-time IAV than its southern counterpart.

Figure 6a is similar to Fig. 4a but for mid-latitude day-time REC data. The SW ratio at northern mid-latitudes is greater than unity during all the years except for 2001 and 2014. While the same ratio at southern counterpart is greater than unity for all the years. The corresponding maximum values are found to occur in the year 2011; at ASML (2.95), AFML (3.94), AMML (4.41) and PAML (3.46). The summer (south) to winter (north) ratio is greater than 1 during all the considered years except during 2000 (ASML region only) and 2001 (ASML and PAML regions only). Figure 6b is similar to Fig. 4b but for night-time mid-latitude REC data. The night-time SW ratio at low-latitude is greater than unity in both hemispheres. However, the said ratio is much higher in the southern regions as compared to northern counterpart. It can be seen that the SW ratio in the southern mid-latitudinal regions follows the solar cycle trend.

3.4 Trends in the IAV at hemispheric, low- and mid-latitude

Figures 7a presents scatter plot of SW ratio against the SSN in four longitudinal sectors, namely Asia (top left), Africa (top right), America (bottom left) and Pacific (bottom right), respectively in the northern hemisphere. On each plot, a linearly fitted curve with its equation is drawn in red. It can be seen that the slope of the said linear equation is negative for all regions having the values of -0.0025, -0.0016, -0.0025 and -0.0029 for Asia, Africa, America and Pacific regions, respectively. The slope is minimum for the Pacific, followed by Asia, America and Pacific, respectively. Figure 7b is similar to Fig. 7a but for day-time southern hemisphere. The slope of fitting curve in this case is negative for Asia and Africa having the respective values -0.0016 and -0.0025. Whereas it is positive for America and Pacific with values 0.0002 and 0.0011, respectively. Figure 8a is similar to Fig. 7a but for night-time data. It can be seen that slope of fitting equation is positive during night-time for all regions. The said slope is maximum for Pacific (m=0.0037), followed by America (m=0.0036), Africa (m=0.0031) and Asia (m=0.008). A similar plot for night-time data of the southern hemisphere is presented in Fig. 8b. The southern hemisphere also exhibit a positive slope for SW ratio and SSN in all regions. However, the value of slope is found to be much higher than norther counterpart. The

numerical values of the said slope, in Asia, Africa, America and Pacific, is found to be 0.0095, 0.0082, 0.0068 and 0.0096, respectively. An analogous examination is also performed for low and low-latitudes for day- and night-time SW ratio. However, due to limitation on maximum number of manuscript figures, those plots are not presented here. The results of low and low-latitudes are found to be consistent with their respective hemispheres, which is consistent with Figs. 7 and 8.

To further analyze the nature and extent of correlation between SW ratio of REC against SSN, we have computed the Pearson correlation (Benesty et al., 2009) for all selected regions during day- and night-time. Figure 9a presents the Pearson correlation (r) of day-time SW ratio for hemisphere (top), low-latitudes (middle) and mid-latitudes (bottom), respectively. On each panel, northern and southern regions are presented, orderly in left and right. The day-time northern hemisphere exhibits a strongly negative correlation with maximum effect in Pacific (r=-0.63), Asia (r=-0.55), America (r=-0.55) and Africa (r=-0.41). On the other hand, the said correlation is found to be weakly negative in Asia (r=-0.24) and Africa(r=-0.32) regions of southern counterpart, while it is positive in America and Pacific regions having correlation 0.02 and 0.188, respectively. Similarly, the low-latitude regions of both hemispheres exhibit similar trends. The low-latitude region also depicts similar trends but with higher magnitude of correlation coefficients.

Figure 9b is similar to Fig. 9a but for night-time SW ratio. It can be noticed that correlation coefficient is positive for all latitudinal regions during the night-time except the Asian region of northern low-latitude. The magnitude of correlation coefficient is >5 for all regions except Asia. This indicates that day-time SW ratio exhibit strong linear dependence on solar activity.

Figure 10a presents the Pearson correlation between SW ratio and sunspot number for four longitudinal sectors of HEC of SC-23 (in blue) and SC-24 (in red), respectively. The top row, from left to right, corresponds to day-time northern and southern HEC, respectively whereas bottom row depicts the results of night-time data. Pearson correlation for day-time SW ratio is negative in northern hemisphere whereas the magnitude of said correlation is high during the SC-23 as compared to SC-24. However, day-time SW ratio depicts the negative correlation for Asia and Africa regions and positive correlation during America and Pacific counterparts. The night-time SW ratio shows that correlation coefficient is high during the SC-23 as compared to SC-24. Figure 10b is similar to Fig. 10a but for low-latitude SW ratio. The results of Pearson correlation for low-latitude SW ratio is similar to HEC during day-time. However, a negative correlation is found for night-time SW ratio of northern part. Figure 10c is similar to Fig. 10a but for mid-latitude REC data. The mid-latitudes SW ratio depicts that magnitude of r is high for SC-23 as compared to SC-24. This

demonstrates the correlation between the intensity of SC and SW ratio. In the next section, we will provide the physical explanation to these results with reference to earlier studies.

4. Discussion

In the preceding section, we presented the annual REC variations globally as well as at low and mid-latitudes. The present section is devoted to discussing the main findings of the present work as follows.

Figures 1, 3 and 5 indicate that there exist a north-south asymmetry in the amplitude of IAV. The southern hemisphere has much higher amplitude than its northern counterpart at most of the considered latitudinal bands. The day- and night-time hemispheric IAV (Fig. 1) manifests that this asymmetry is maximum for the Pacific region, followed by America, Africa and Asia hemispheric regions, respectively. Moreover, at low-latitude, we observe that this asymmetry follows the same trend during day-time whereas at night-time it is maximum for Asia, followed by Africa, America and Pacific, respectively (Figs. 3a and b). The day-time IAV at mid-latitude regions exhibit the same pattern in the amplitude as observed for low-latitudes counterparts. Whereas, the night-time IAV at Asian and African mid-latitudes have higher amplitude at northern hemisphere. This asymmetry in the amplitude of IAV can be associated with the phenomenon of annual asymmetry and winter anomaly (Torr & Torr, 1973). The effect of annual asymmetry is in-phase (out-phase) for the southern (northern) hemisphere. Hence, this enhances the amplitude of IAV at southern hemisphere and suppresses the same in northern hemisphere (Liu et al., 2003; Yasyukevich et al., 2018; Zhao et al., 2007). The longitudinal variation of hemispheric asymmetry can be related to the variations in the strength of winter anomaly, which is stronger in the north American and south Australian sectors. This eventually leads to hemispheric asymmetry in the amplitude of IAV which is maximum for Pacific, followed by America, Africa and Asia, respectively (Zou et al., 2000; Rishbeth et al., 2000). Yue et al. (2019) and Qian et al. (2023) reported the annual oscillation in thermospheric composition using the GUVI data. The variation in the Sun-earth distance cannot completely explain the origin of annual variations and it is suggested that the vary Sun-Earth distance accounts for ~67% of the annual oscillation in the thermosphere density, while rest of it may be developed from the lower atmosphere (Lei et al. 2013). Comparison of thermospheric and ionospheric features for annual variations with modeled simulation leads to the conclusion that the distribution of lands and oceans is different between both hemispheres. The excitation, propagation, and dissipation of atmospheric waves (gravity waves, planetary waves, and tides) can have strong hemispheric asymmetry which may affect the amplitude of annual oscillations in both hemispheres (Qian et al., 2009).

The IAV are regular, during day- and night-time in the southern hemisphere of all the longitudinal sectors (Fig. 1). In this regard, the northern hemisphere manifests complicated variations during the day-time. During the peak of SC-23, AIAV is observed at all considered sectors. However, phase of IAV in the northern hemisphere varies with the intensity of SC and its peak tends to shift towards local summer as one approaches to solar minimum. Whereas, during night-time, the northern hemisphere exhibits RIAV at all considered longitudinal sectors. The day-time SW ratio of REC in the northern hemisphere is also less than unity during the years 2001, 2011, 2014 and 2020. The night-time ratio of REC follows the SC and becomes almost equal to unity during the solar minimum.

The northern low-latitudes exhibit a day-time AIAV at all longitudes and its amplitudes varies with the SC. During night-time, we see AIAV at northern low-latitudes in the years of solar minimum having a maximum amplitude for Pacific sector (Figure 3). The same can also be verified by SW ratio as depicted in Fig. 4; the said ratio during the night-time in the northern hemisphere follows the solar activity and exhibits a minimum value in the years of solar minimum. The AIAV at low-latitudes during the night-time are evident in deep solar minimum between SC-23 and 24. At mid-latitudes, it can be seen that the northern hemisphere exhibits AIAV during the peak of SC-23, but it tends to shift towards the RIAV as intensity of solar activity decreases. The amplitude of IAV in the southern hemisphere varies with solar activity and its amplitude remains high during the peak of SC-23 as compared to SC-24. This trend is also observed in low- and mid-latitude regions of the southern hemisphere. On the other hand, the IAV in the northern hemisphere are less influenced by solar activity. Jakowski et al. (2015) reported the existence of night-time AIAV in the Asian region of southern mid latitude regions. However, this trend has not been observed in the present work, where the said variations are detected in the northern hemisphere only. Moreover, we note that the SW ratio for the ASML decreases during the years of low solar activity but did not reach less than unity. The apparent contradiction with finding of Jakowski et al. (2015) may be associated with different parameters and techniques used in both works. Earlier studies (Jakowski et al., 2015) reported the existence of nigh-time AIAV only in the mid latitude of American longitude, whereas we have noticed that night-time AIAV can be observed over wider longitudes from Africa to America at mid and low latitudes. Such expansion of night-time AIAV to wider longitude (and latitude) regions has also been reported by some recent studies (Wang et al.,2021; Meza & Fernández, 2012). The linear fitting (Fig. 7) and Pearson correlation (Fig. 9a) of day-time SW ratio against SSN manifest a negative correlation, i.e., the SW ratio during day-time decreases with increasing solar activity. Moreover, the said correlation and slope of fitting equation is larger in the northern regions as compared to southern counterparts. As a result of this difference, the SW ratio becomes less than

unity under a high solar activity. This corresponds to anomalous ionospheric behaviors, i.e., winter has higher electron content than summer season. The fitting curve depicts that the day-time winter anomaly can be detected in the northern hemisphere for SSN>120. This trend is in agreement with the findings of Burns et al. (2013), who investigated the variations of winter anomaly and reported that it is maximum during the peak of a SC. The changes in the intensity of winter anomaly can be associated with seasonal variations of O/N_2 which are high (low) during the solar maximum (minimum). The stronger winter anomaly in the northern hemisphere may be associated with the annual asymmetry, which states that December has high ionospheric plasma density as compared to June (Mikhailov & Perrone, 2011).

The linear fitting (Fig. 8) and Pearson correlation (Fig. 9b) of night-time SW ratio against SSN demonstrate a positive correlation in both hemispheres for all regions except Asia. Contrary to day-time, the night-time anomaly – when the SW ratio becomes less than unity – can only be present under a low solar activity. The increase in the intensity of night-time ionospheric anomaly during a solar minimum has also been reported by Jakowski et al. (2015) and Wang et al. (2021).

5. Summary

In this paper, we have investigated the features of IAV during the solar cycles 23 and 24, for both hemispheres, in four longitudinal sectors (Asia, Africa, America and Pacific) using the REC. For that we have used REC data of the five magnetic quiet days of each month for mid- and low-latitudes. The regular IAV (RIAV) corresponds to the conditions in which REC value for summer is greater than its winter counterpart, while an opposite trend holds true for the anomalous IAV (AIAV). The main findings of our studies are summarized as follows.

1. There exists a hemispheric asymmetry in the amplitude of IAV, which is maximum for the Pacific sector, followed by America, Africa and Asia (Figs. 1,3 and 5).
2. The southern hemisphere exhibits RIAV during the considered period in both day- and night-time (Figs. 1,3 and 5).
3. The SW ratio – during day- and night-time – in the southern hemispheric region is always greater than unity during solar cycles 23 and 24 (Fig. 2).
4. The phase of day-time IAV in the northern hemisphere varies with the SC. During the years of solar maxima, the positive and negative peaks of day-time IAV are observed, respectively in local winter and summer. However, with the decrease in level of solar activity, peaks tend to shift towards local summer and winter, respectively (Figs. 1, 3 and 5).

5. The night-time IAV in the northern hemispheric regions manifest a counter trend as compared to day-time. The RIAV are observed during the peaks of SC-23 and 24, however it tends to exhibit AIAV during the period of solar minimum.

6. The night-time SW ratio in the northern region – during the peak years of SC-23 and 24 – is much greater than unity. Furthermore, the said ratio approaches to unity in the years of deep solar minimum.

7. The day-time SW ratio decreases strongly with the SC in the northern hemisphere, whereas the corresponding ratio has small variation in the southern hemisphere (Fig. 7).

8. The day-time SW ratio can become less than unity in the northern hemisphere when SSN >120.

9. The night-time SW ratio shows an enhancement with intensity of SC at both hemispheres. Hence, winter anomaly in night-time ionosphere can be observed in the years of solar minimum (Fig. 8).

Acknowledgement

This research work was supported by the Higher Education Commission (HEC) of Pakistan through NRPU project No 20-14405/NRPU/R&D/HEC/2021 titled “Space weather effects on ionosphere”. The authors are thankful to the IGS Community for providing GNSS data, OMNI web data center (http://omniweb.gsfc.nasa.gov/) for making available solar indices. The SEM/SOHO EUV data are downloaded from the Web site http://www.usc.edu/ dept/space_science/semdatafolder/long/. The CELIAS/ SEM experiment on the Solar Heliospheric Observatory (SOHO) spacecraft (SOHO is a joint European Space Agency, U.S. National Aeronautics and Space Administration mission). The 10.7 cm solar radio flux data are provided as a service by the National Research Council of Canada. We thank the SDO/AIA instrument team for providing the coronal observations. C. Ammory-Mazaudier thank the ISSI-Bern International Team of ‘Why Ionospheric Dynamics and Structure Behave Differently in The African Sector? (The team leaders E. Yizengaw & K. Groves) for a valuable discussion about part of the result that is included in this paper.

References

Azpilicueta, F., & Nava, B. (2021). A different view of the ionospheric winter anomaly. Advances in Space Research. Elsevier BV. https://doi.org/10.1016/j.asr.2020.10.039

Béniguel, Y., Cherniak, I., Garcia-Rigo, A., Hamel, P., Hernández-Pajares, M., Kameni, R., et al. (2017, March 13). MONITOR Ionospheric Network: two case studies on scintillation and electron content variability. Annales Geophysicae. Copernicus GmbH. https://doi.org/10.5194/angeo-35-377-2017

Benesty, J., Chen, J., Huang, Y., & Cohen, I. (2009). Pearson correlation coefficient. In Noise reduction in speech processing (pp. 37–40). Springer.

Burns, A. G., Wang, W., Qian, L., Solomon, S. C., Zhang, Y., Paxton, L. J., & Yue, X. (2014, June). On the solar cycle variation of the winter anomaly. Journal of Geophysical Research: Space Physics. American Geophysical Union (AGU). https://doi.org/10.1002/2013ja019552

Jakowski, N., R. Landrock, and A. Jungstand (1990), The Nighttime Winter Anomaly (NWA) effect at the Asian longitude sector, Gerl. Beitr. Geophys., 99, 163–168.

Jakowski, N., Hoque, M.M., Kriegel, M., Patidar, V., 2015. The persistence of the NWA effect during the low solar activity period 2007–2009. J. Geophys. Res. Space Phys. 120, 9148–9160. https://doi.org/10.1002/2015JA021600

Karia, S. P., Kim, J., Afolayan, A. O., & Lin, T. I. (2019, March). A study on Nighttime Winter Anomaly (NWA) and other related Mid-latitude Summer Nighttime Anomaly (MSNA) in the light of International Reference Ionosphere (IRI) – Model. Advances in Space Research. https://doi.org/10.1016/j.asr.2018.11.021

Liu, J. Y., Y. I. Chen, and J. S. Lin (2003), Statistical investigation of the saturation effect in the ionospheric foF2 versus sunspot, solar radio noise, and solar EUV radiation, J. Geophys. Res., 108(A2), 1067, doi:10.1029/2001JA007543

Lei, J., Dou, X., Burns, A., Wang, W., Luan, X., Zeng, Z., & Xu, J. (2013). Annual asymmetry in thermospheric density: Observations and simulation. Journal of Geophysical Research: Space Physics, 118, 2503–2510. https://doi.org/10.1002/jgra.50253

Mikhailov AV, Perrone L. 2011. On the mechanism of seasonal and solar cycle N m F2 variations: A quantitative estimate of the main parameters contribution using incoherent scatter radar observations. J. Geophys. Res. 116: A03319. DOI: 10.1029/2010JA016122

Meza, A., Natali, M. P., & Fernández, L. I. (2012, January). Analysis of the winter and semiannual ionospheric anomalies in 1999-2009 based on GPS global International GNSS Service maps. Journal of Geophysical Research: Space Physics. American Geophysical Union (AGU). https://doi.org/10.1029/2011ja016882

Qian, L., Yu, W., Pedatella, N., Yue, J., & Wang, W. (2023, May). Hemispheric Asymmetry of the Annual and Semiannual Variation of Thermospheric Composition. Journal of Geophysical Research: Space Physics. American Geophysical Union (AGU). https://doi.org/10.1029/2022ja031077

Qian, L., Solomon, S. C., & Kane, T. J. (2009). Seasonal variation of thermospheric density and composition. Journal of Geophysical Research, 114, A01312. https://doi.org/10.1029/2008JA013643

Rishbeth H. 1998. How the thermospheric circulation affects the ionosphere. J Atm Sol-Terr Phys 60: 1385–1402. DOI: 10.1016/S1364-6826(98)00062-5.

Rishbeth, H., & Müller-Wodarg, I. C. F. (2006, December 21). Why is there more ionosphere in January than in July? The annual asymmetry in the F2-layer. Annales Geophysicae. Copernicus GmbH. https://doi.org/10.5194/angeo-24-3293-2006

Rishbeth, H., 2007, Thermospheric targets, Eos Trans. AGU, 88(17), 189

Torr MR, Torr DG. 1973. The seasonal behaviour of the F2-layer of the ionosphere. J Atm Terr Phys 35: 2237–2251. DOI: 10.1016/0021-9169(73)90140-2.

Wang, X., Yang, D., He, H., Zhao, G., Guo, F., Zhou, N., & Jiang, W. (2021, December). The nighttime winter anomaly phenomenon observed by the in situ electron density measurements from the CSES satellite. Advances in Space Research. Elsevier BV. https://doi.org/10.1016/j.asr.2021.09.033

Yasyukevich, Yu.V., Yasyukevich, A.S., Zhfvetiev, I.V., 2018. Global Electron Content in the 23rd and 24th Solar Cycles. 2018 Progress in Electromagnetics Research Symposium (PIERS-Toyama). IEEE. https://doi.org/10.23919/piers.2018.8597938.

Yasyukevich Y, Yasyukevich A, Ratovsky K, Klimenko M, Klimenko V, et al. 2018. Winter anomaly in NmF2 and TEC: when and where it can occur. J. Space Weather Space Clim. 8, A45.

Younas, W., Amory-Mazaudier, C., Khan, M., & Amaechi, P. O. (2023, January). Climatology of global, hemispheric and regional electron content variations during solar cycles 23 and 24. Advances in Space Research. Elsevier BV. https://doi.org/10.1016/j.asr.2022.07.029

Yue, J., Jian, Y., Wang, W., Meier, R. R., Burns, A., Qian, L., et al. (2019, April). Annual and Semiannual Oscillations of Thermospheric Composition in TIMED/GUVI Limb Measurements. Journal of Geophysical Research: Space Physics. American Geophysical Union (AGU). https://doi.org/10.1029/2019ja026544

Zou L, Rishbeth H, Müller-Wodarg ICF, Aylward AD, Millward GH, Fuller-Rowell TJ, Idenden DW, Moffett RJ. 2000. Annual and semiannual variations in the ionospheric F2-layer. I. Modelling. Ann Geophys 18: 927–944. DOI: 10.1007/s00585-000-0927-8

Zhao, B., Wan, W., Liu, L., Mao, T., Ren, Z., Wang, M., Christensen, A. B., 2007. Features of annual and semiannual variations derived from the global ionospheric maps of total electron content. Ann. Geophys. 25, 2513–2527. https://doi.org/10.5194/angeo-25-2513-2007.

Table Caption

Table 1: The geographic limits of different longitudinal regions used in this work.

Table 2: The main characteristics of solar cycles 23 and 24.

Figure Captions

Figure 1: **a)** Day-time ionospheric annual variations in the four longitudinal sectors, from top to 4th panel, Asia, Africa, America and Pacific, respectively for the period 1999 to 2020. On each panel, red (blue) line corresponds to northern (southern) hemisphere. The fifth panel depicts the SSN (blue) and F10.7 (red) index for the same period, respectively. **b)** Similar to Fig. 1a but for night-time ionospheric annual variations.

Figure 2: **a)** Day-time ratio of SW in northern hemisphere (top), SW in southern hemisphere (middle) and summer of southern hemisphere to winter of northern hemisphere (bottom) from 1999 to 2020, respectively. On each panel, the blue, yellow, green and violet colors correspond, orderly to Asia, Africa, America and Pacific. **b)** Similar to Fig. 2a but for night-time variations.

Figure 3: **a)** Day-time IAV at four longitudinal sectors, namely ASLL, AFLL, AMLL and PALL. On each panel the red (blue) line corresponds to the northern (southern) hemispheric region.

Figure 3: **b)** Similar to Fig. 3a but for night-time REC.

Figure 4: **a)** Top to bottom panels presents the ratio of day-time SW ratio of REC in northern low-latitude region, ratio of day-time SW ratio of REC in southern low-latitude sector and ratio of day-time summer (south) to winter (north) REC, respectively.

Figure 4: **b)** Similar to Fig. 4a but for night-time REC.

Figure 5: **a)** Similar to Fig. 3a but for mid-latitudes.

Figure 5: **b)** Similar to Fig. 3b but for mid-latitude regions.

Figure 6: **a)** Similar to Fig. 4a but for mid-latitude day-time REC data.

Figure 6: **b)** Similar to Fig. 4b but for mid-latitude night-time REC data.

Figure 7: a) Scatter plot of annually averaged day-time SW ratio of REC and SSN for Asia (top left), Africa (top right), America (bottom left) and Pacific (bottom right). On each panel, a linear fitting curve with fitting equation is drawn.

Figure 7: b) Similar to Fig. 7a but for the southern hemisphere.

Figure 8: a) Similar to Fig. 7a but for the night-time REC.

Figure 8: b) Similar to Fig. 7b but for the night-time REC.

Figure 9: a) Pearson correlation between sunspot number and day-side SW ratio of – from top to bottom – hemispheric, low and mid-latitudes REC. On each panel, blue, red, yellow and purple bars correspond to Asia, Africa, America and Pacific, respectively.

Figure 9: b) Similar to Fig. 8a but for the night-time REC.

Figure 10: a) Pearson correlation between SSN and hemispheric REC. (Top left panel) day-time North hemisphere, (top right panel) day-time South hemisphere, (bottom left panel) night-time North hemisphere and (bottom right panel) night-time South hemisphere. On each panel, blue and red bars correspond to SC-23 and SC-24, respectively.

Figure 10: b) Similar to Fig. 10a but for low-latitudes.

Figure 10: c) Similar to Fig. 10c but for mid latitudes.

Region	Hemisphere	Latitude	Longitude
Asia	North	0:90	60:150
	South	-90:0	60:150
Africa	North	0:90	-30:60
	South	-90:0	-30:60
America	North	0:90	-120:-30
	South	-90:0	-120:-30
Pacific	North	0:90	-180:-120 & 150:180
	South	-90:0	-180:-120 & 150:180
Asia Low Latitude (ASLL)	North	0:30	60:150
	South	-30:0	60:150
Africa Low Latitude (AFLL)	North	0:30	-30:60
	South	-30:0	-30:60
America Low Latitude (AMLL)	North	0:30	-120:-30
	South	0:30	-120:-30
Pacific Low Latitude (PALL)	North	0:30	-180:-120 & 150:180
	South	-30:0	-180:-120 & 150:180
Asia Mid Latitude (ASML)	North	30:60	60:150
	South	-60:-30	60:150
Africa Mid Latitude (AFML)	North	30:60	-30:60
	South	--60:-30	-30:60
America Mid Latitude (AMML)	North	30:60	-120:-30
	South	-60:-30	-120:-30
Pacific Mid Latitude (PAML)	North	30:60	-180:-120 & 150:180
	South	-60:-30	-180:-120 & 150:180

Table 1

Solar Cycle	Rising Phase	Maximum Phase	Declining Phase	Solar Minimum
23		2000-2002	2003-2005	2006-2009
24	2010-2011	2012-2014	2015-2016	2017-2019

Table 2

Declaration of Interest Statement

The authors declare that they have no conflict of interest

Figure 1a

Click here to access/download;Figure;Figure_1a.jpg

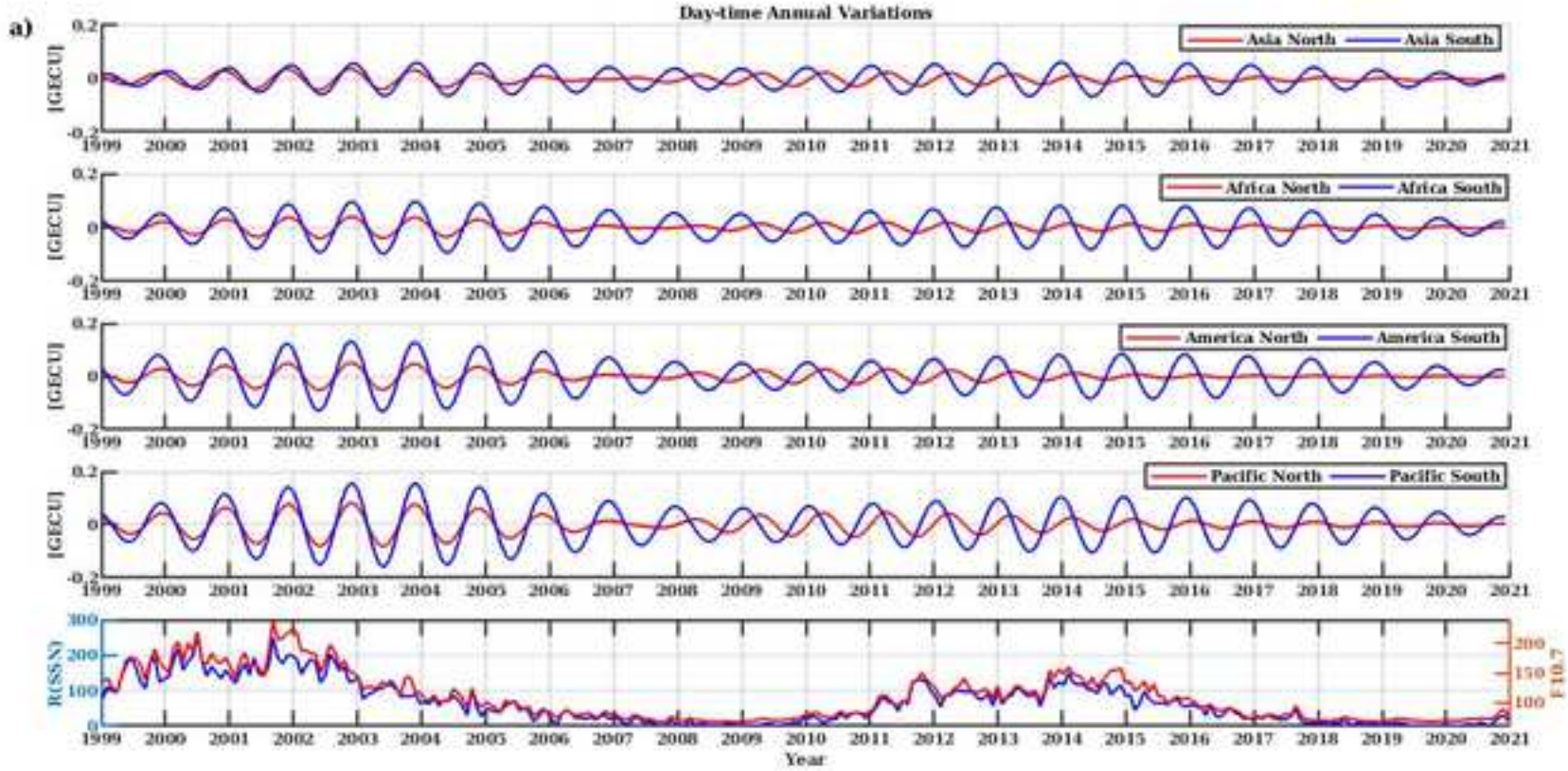

Figure 1b

Click here to access/download;Figure;Figure_1b.jpg

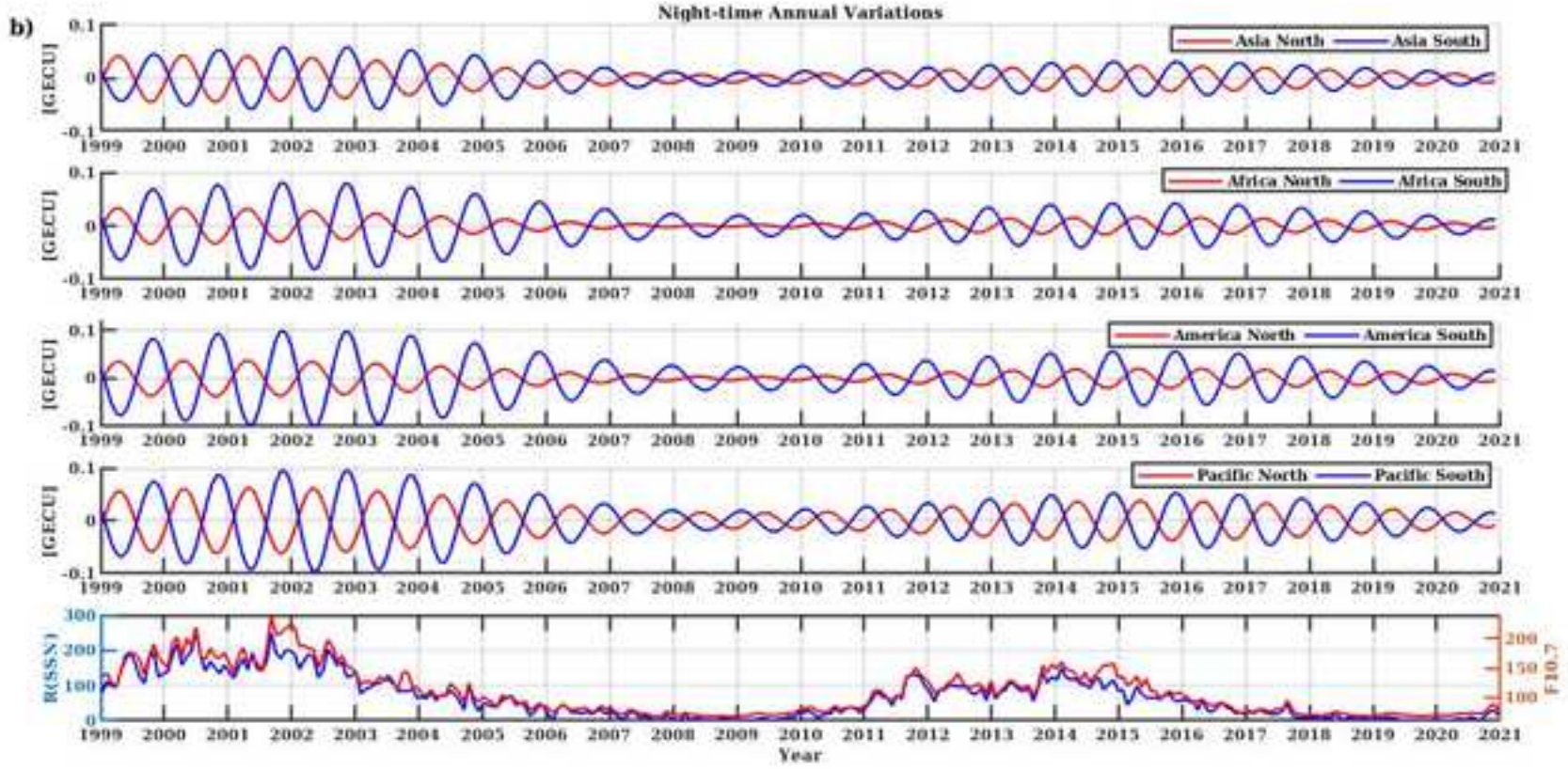

Figure 2a

Click here to access/download;Figure;Figure_2a.jpg

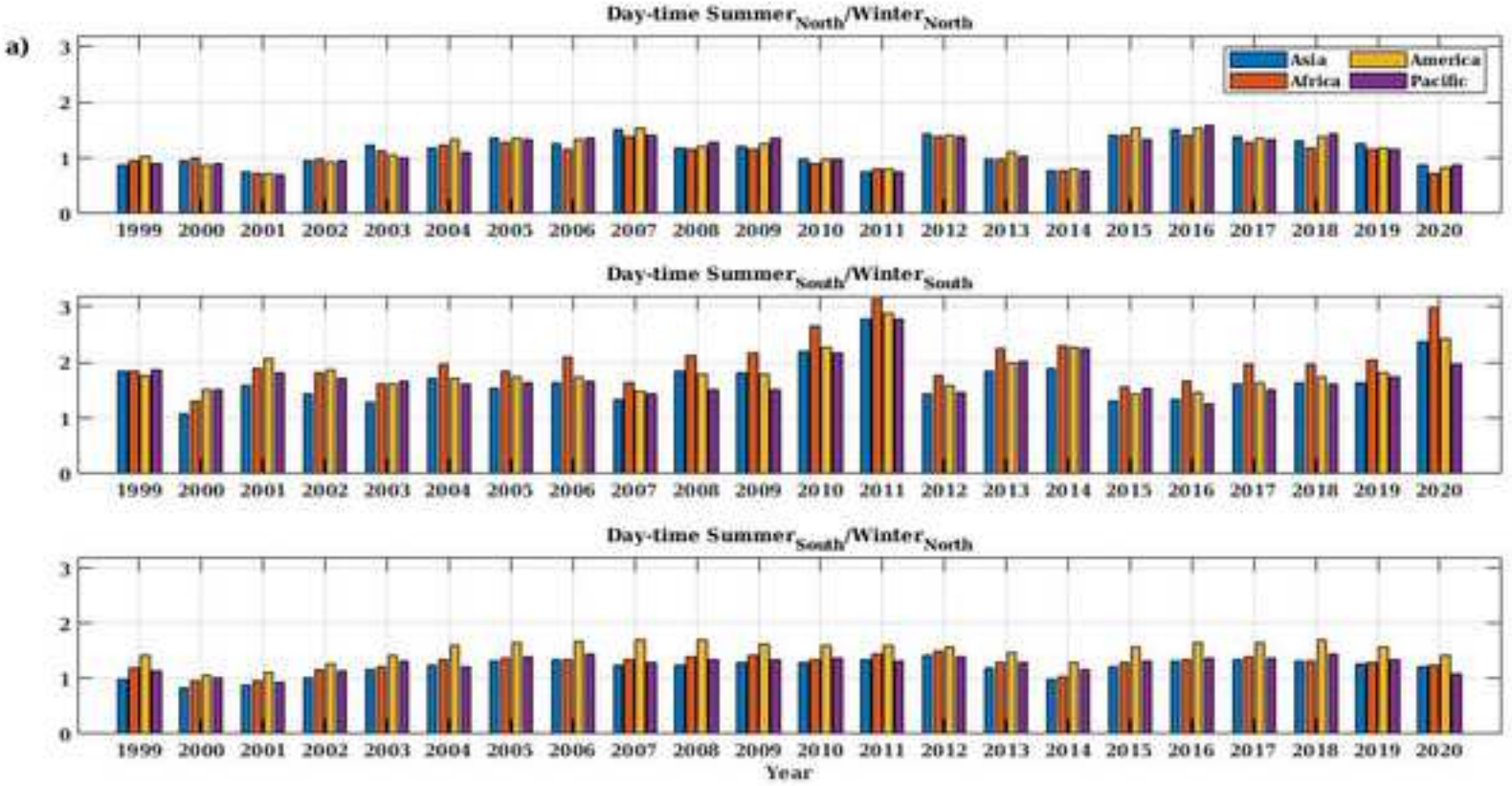

Figure 2b

Click here to access/download;Figure;Figure_2b.jpg

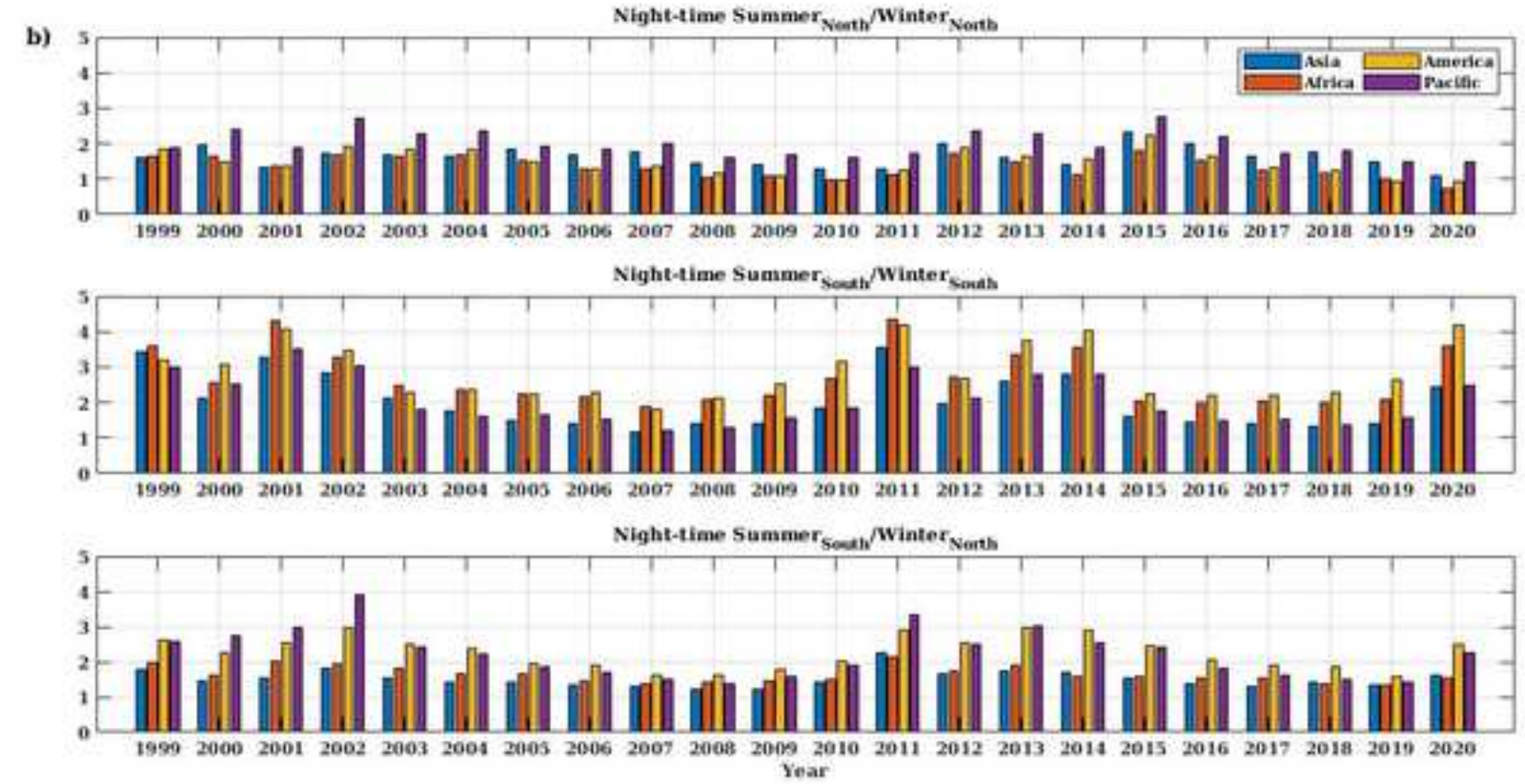

Figure 3b

Click here to access/download;Figure;Figure_3b.jpg

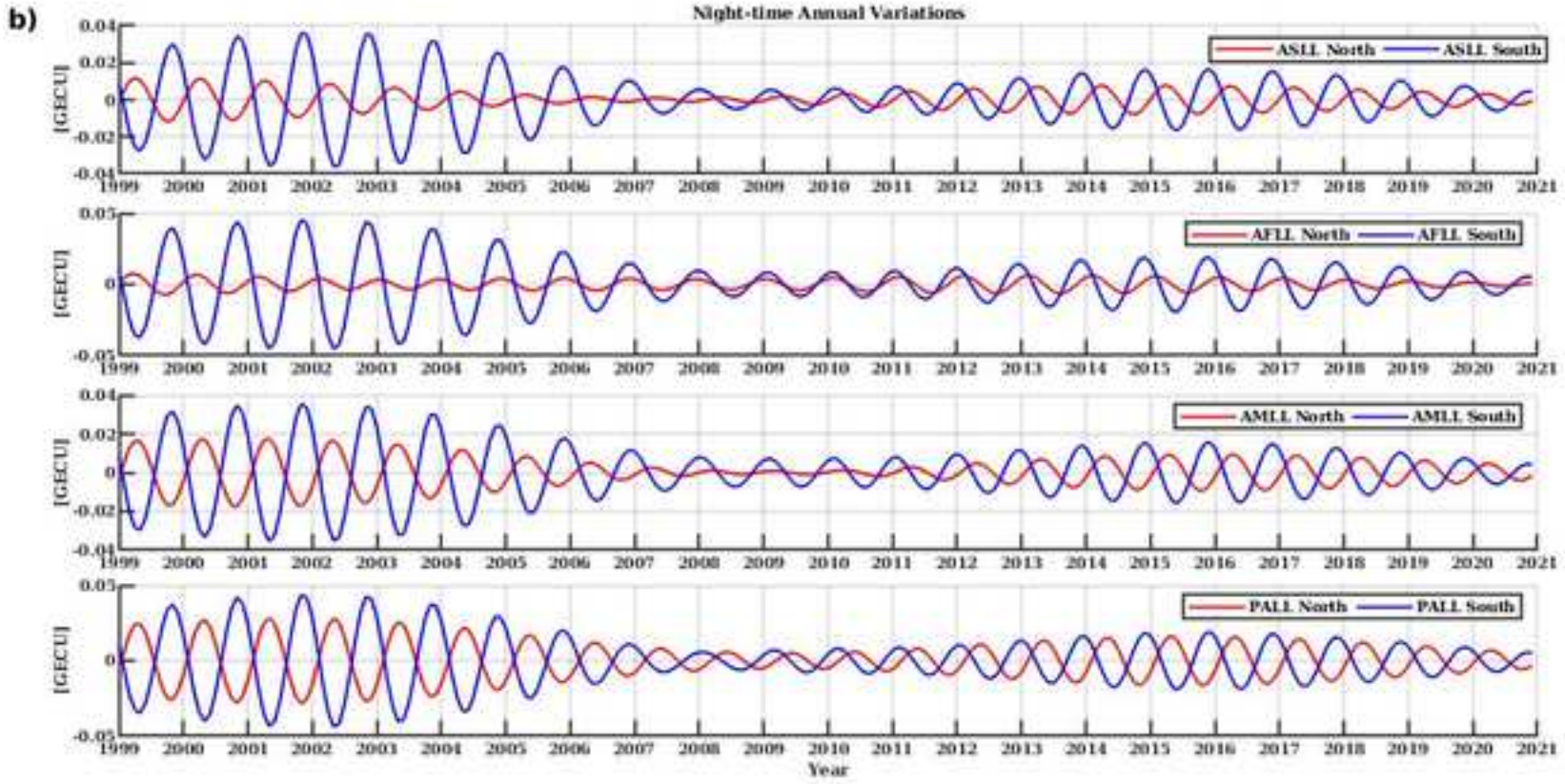

Figure 3a

Click here to access/download;Figure;Figure_3a.jpg

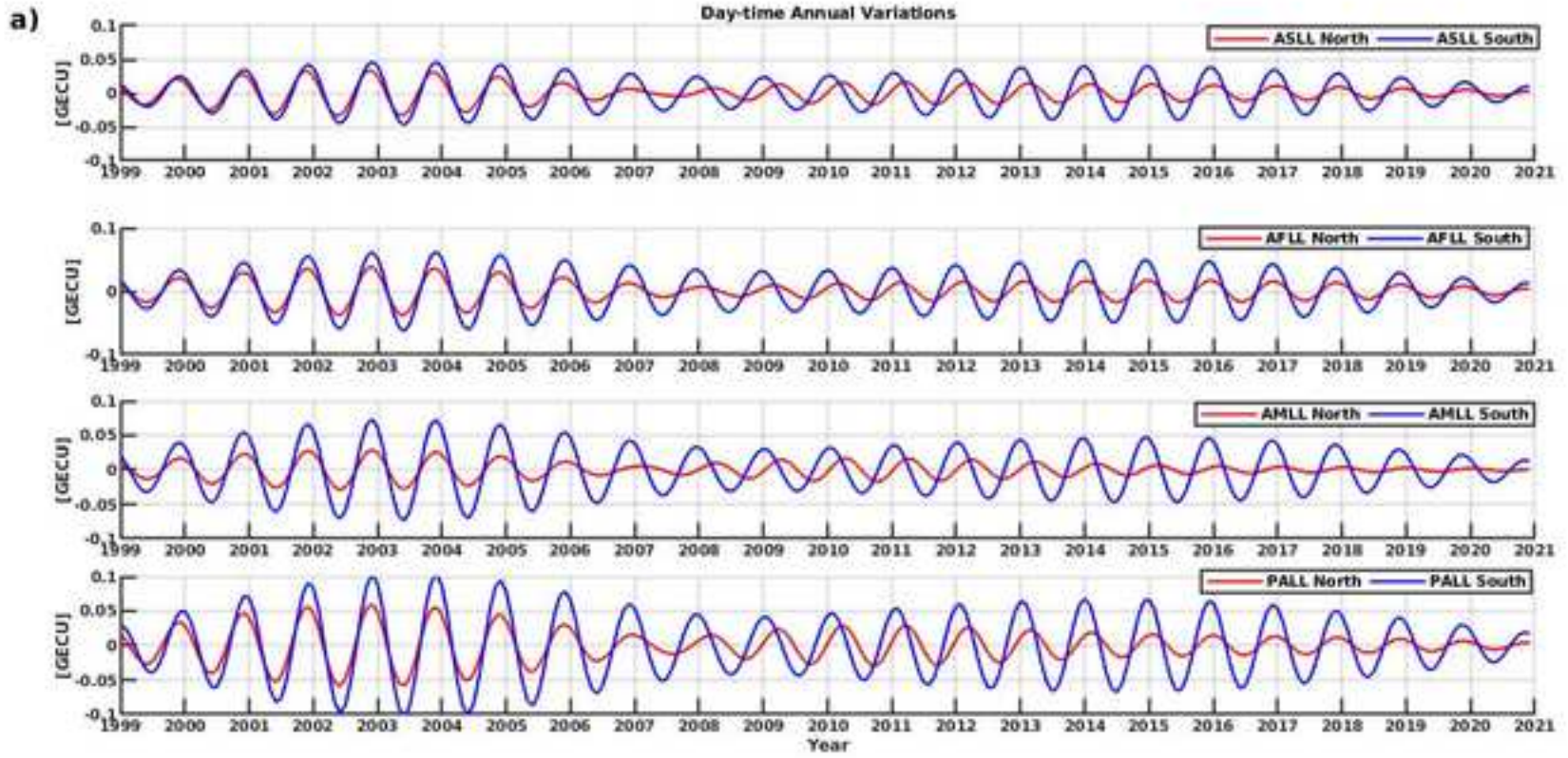

Figure 4a

Click here to access/download;Figure;Figure_4a.jpg

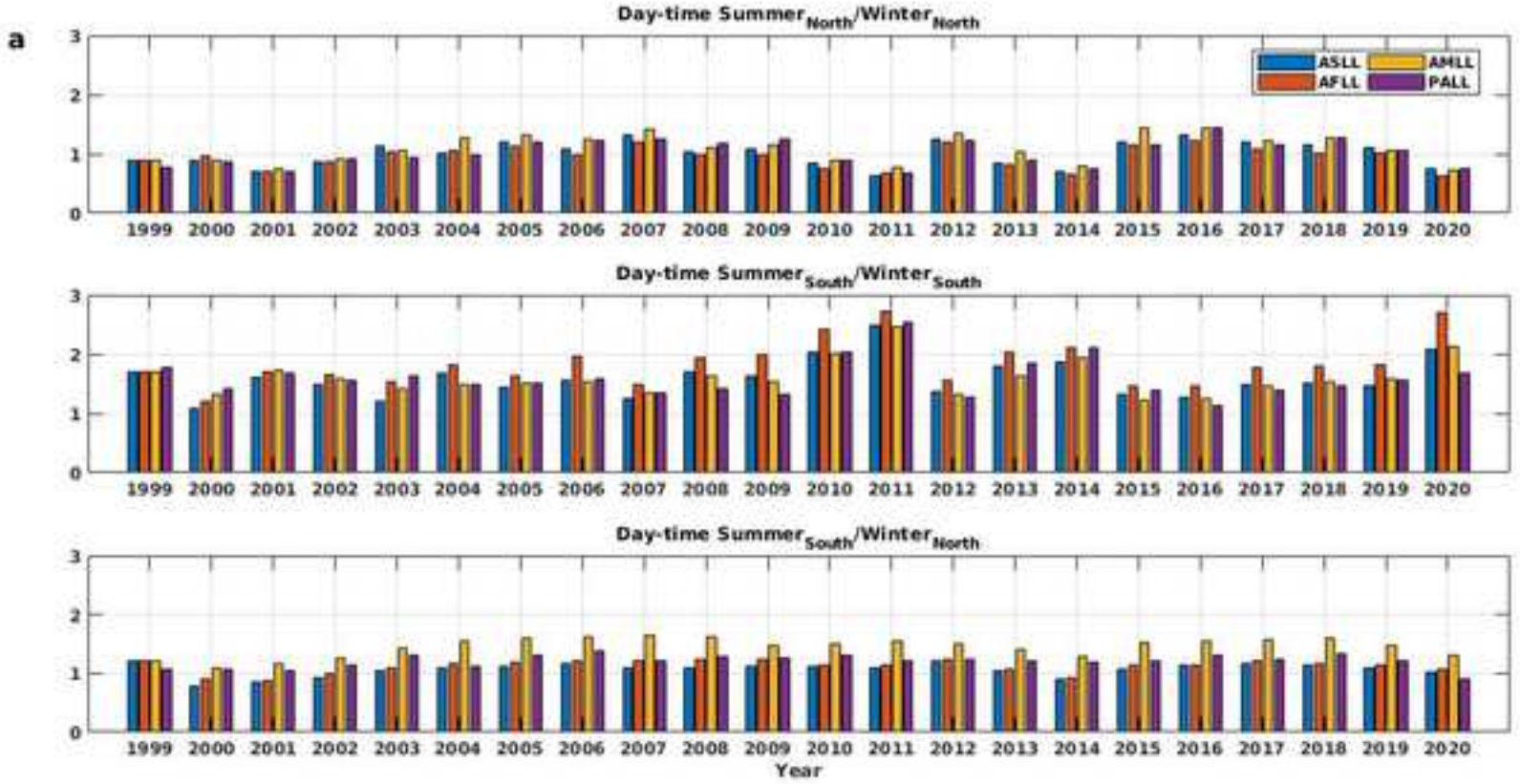

Figure 4b

Click here to access/download;Figure;Figure_4b.jpg

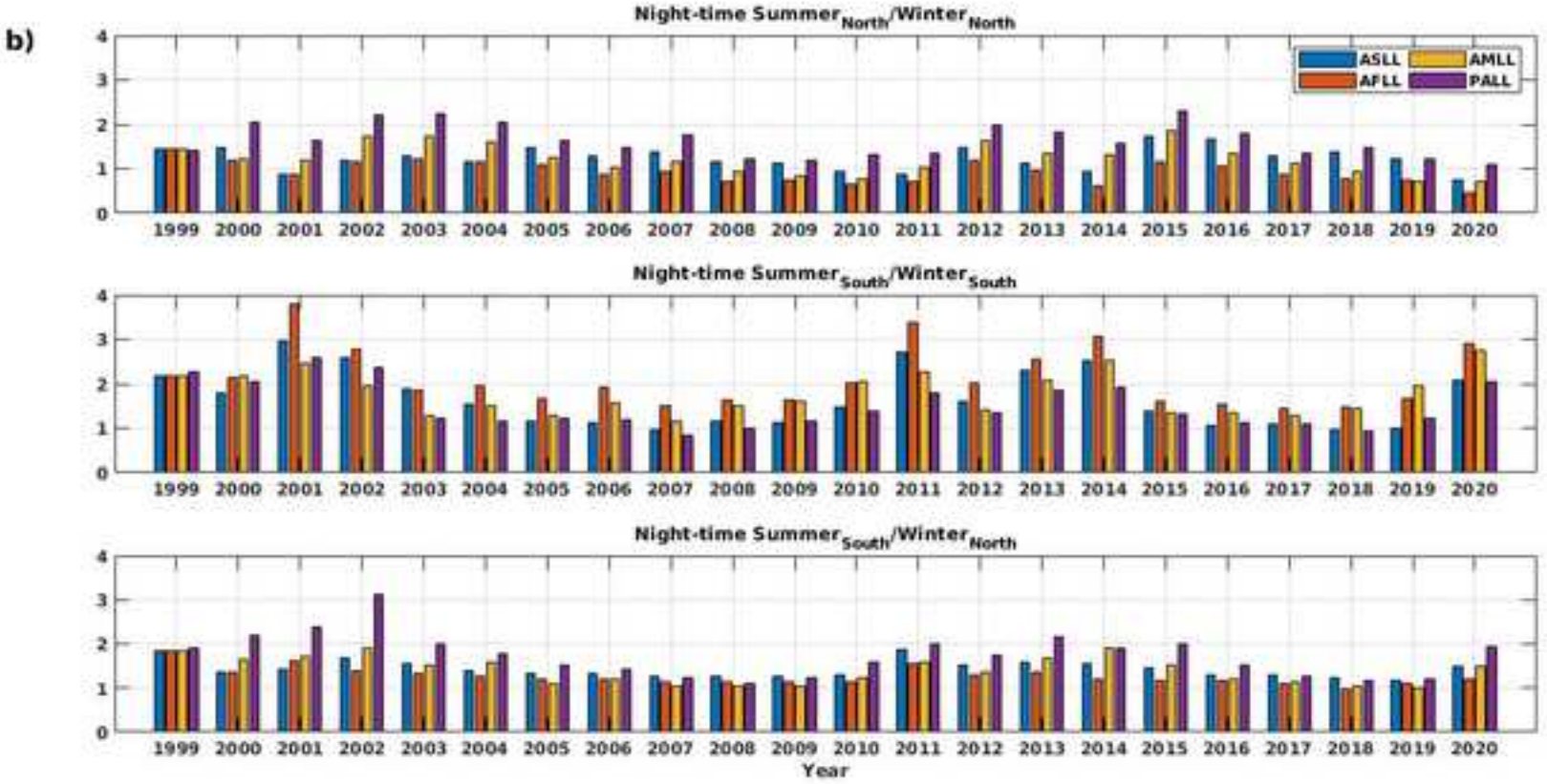

Figure 5a

Click here to access/download;Figure;Figure_5a.jpg

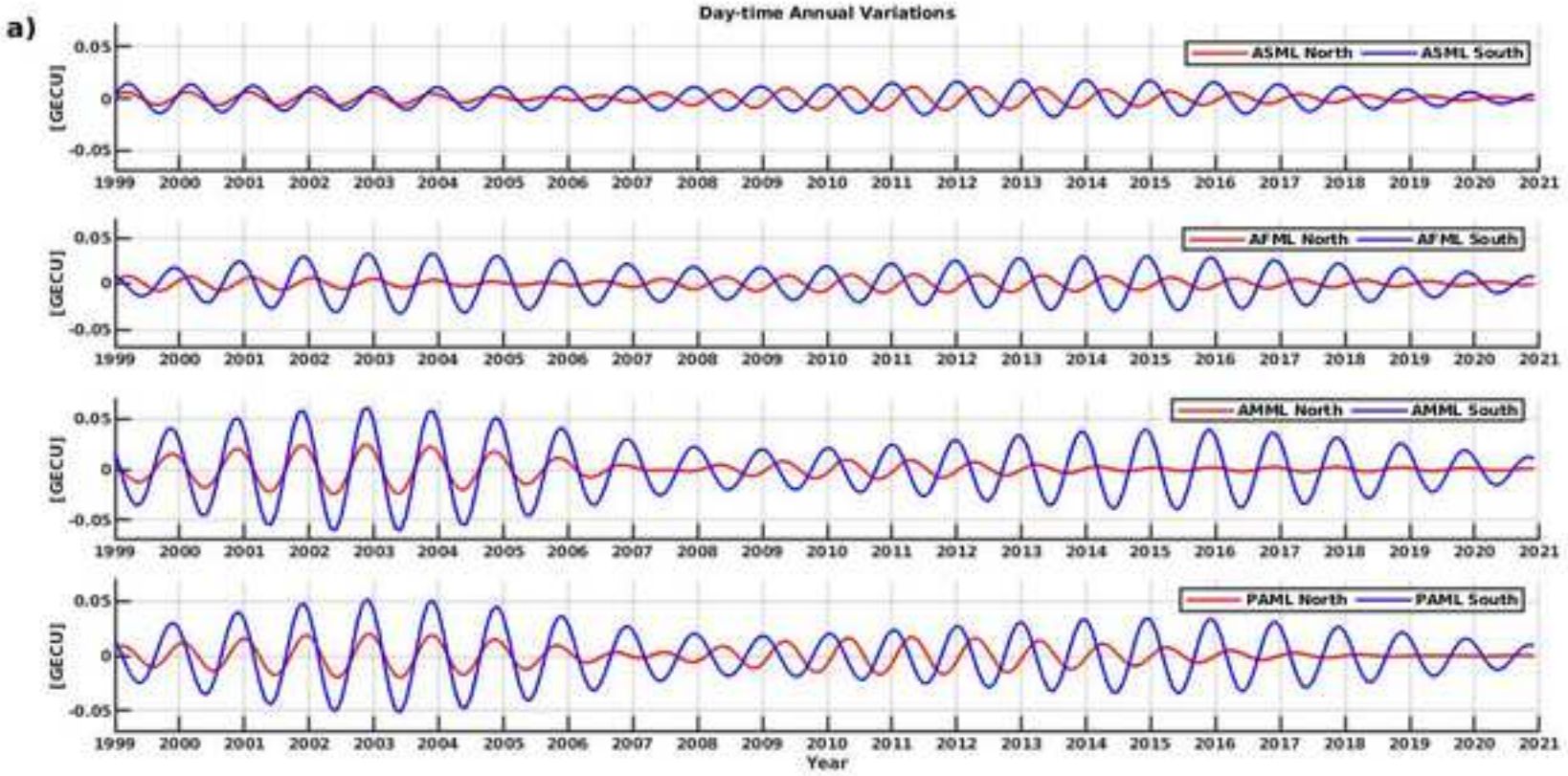

Figure 5b

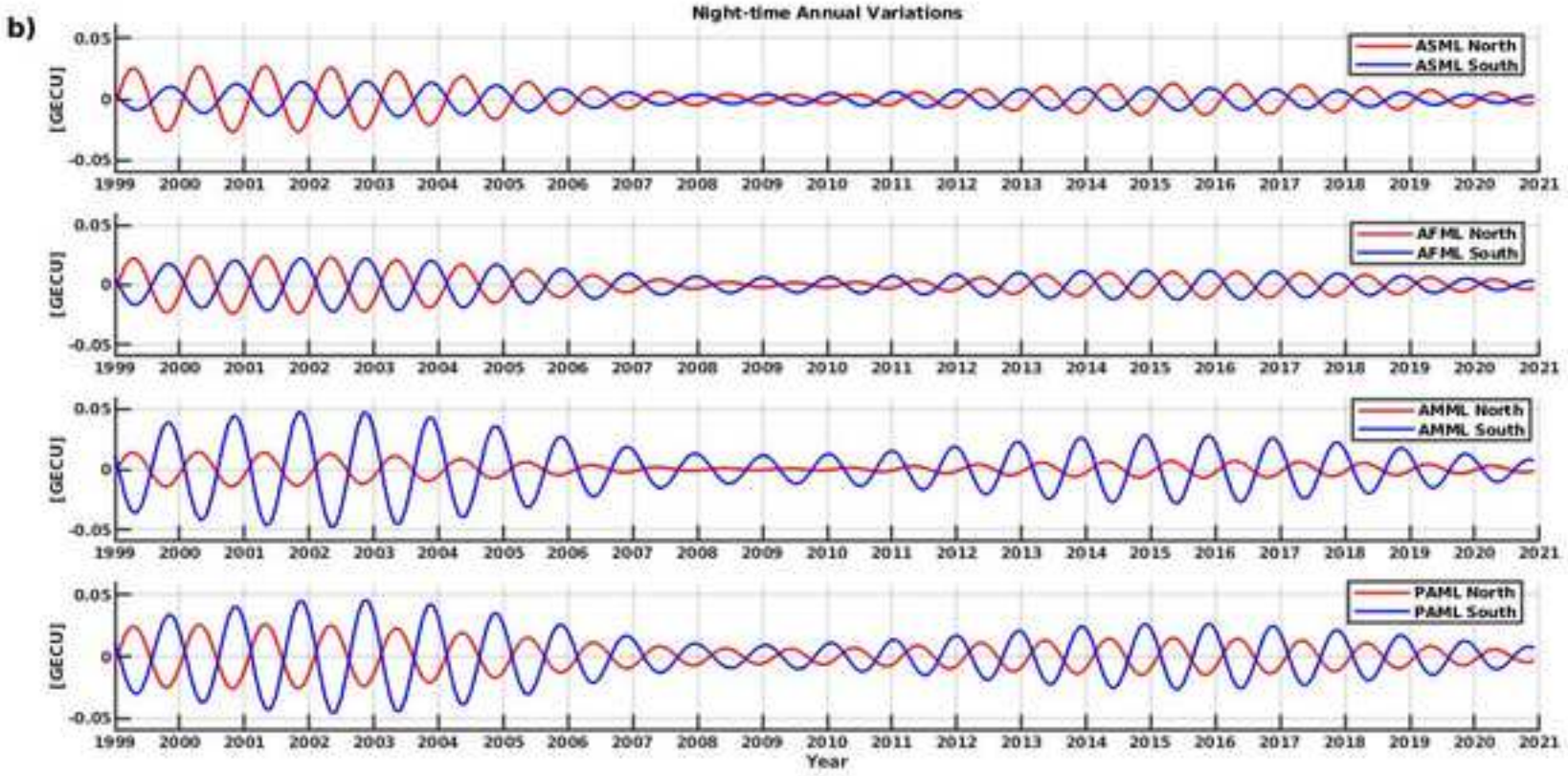

Figure 6b

Click here to access/download;Figure;Figure_6b.jpg

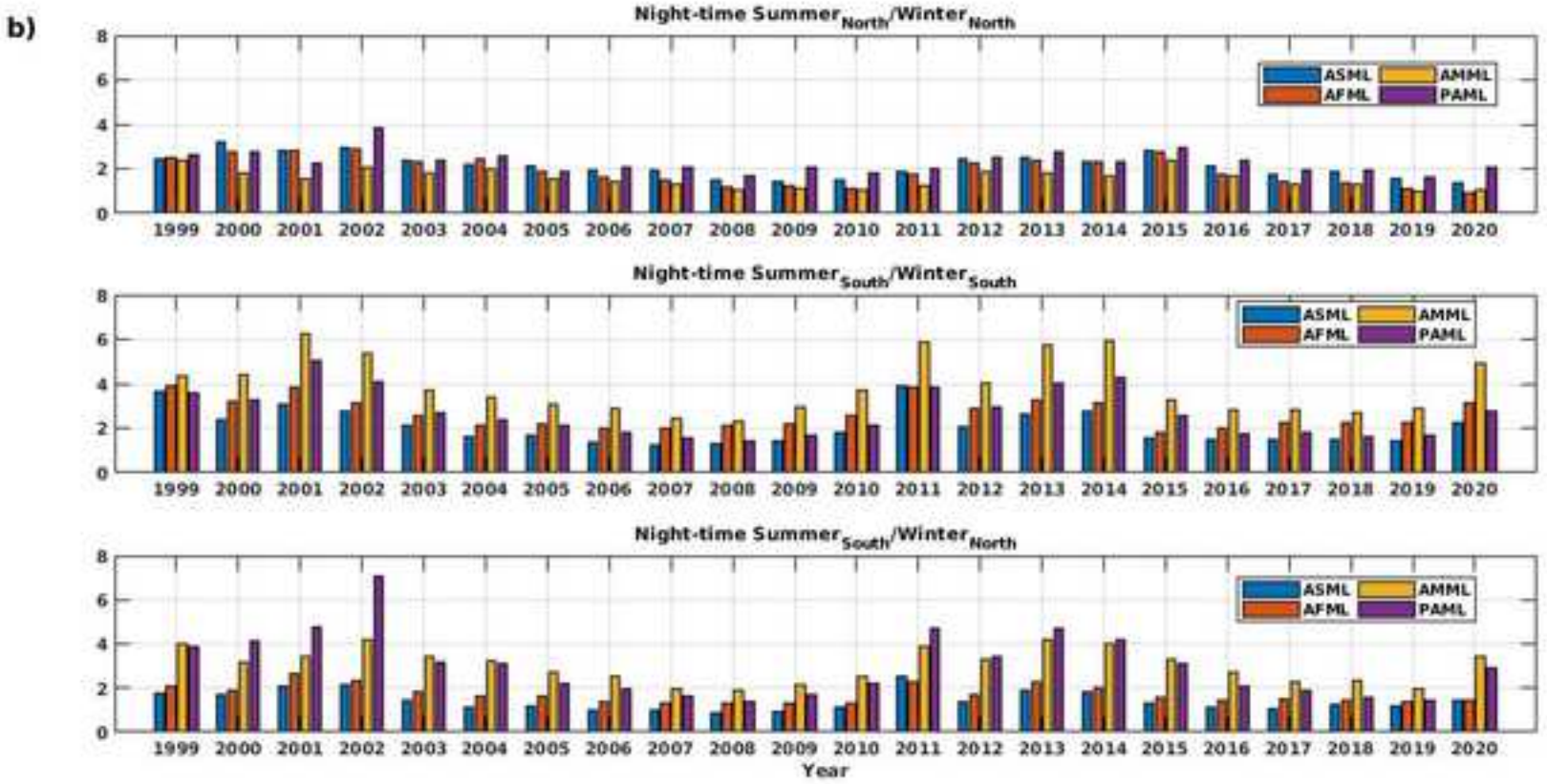

Figure 6a

Click here to access/download;Figure;Figure_6a.jpg

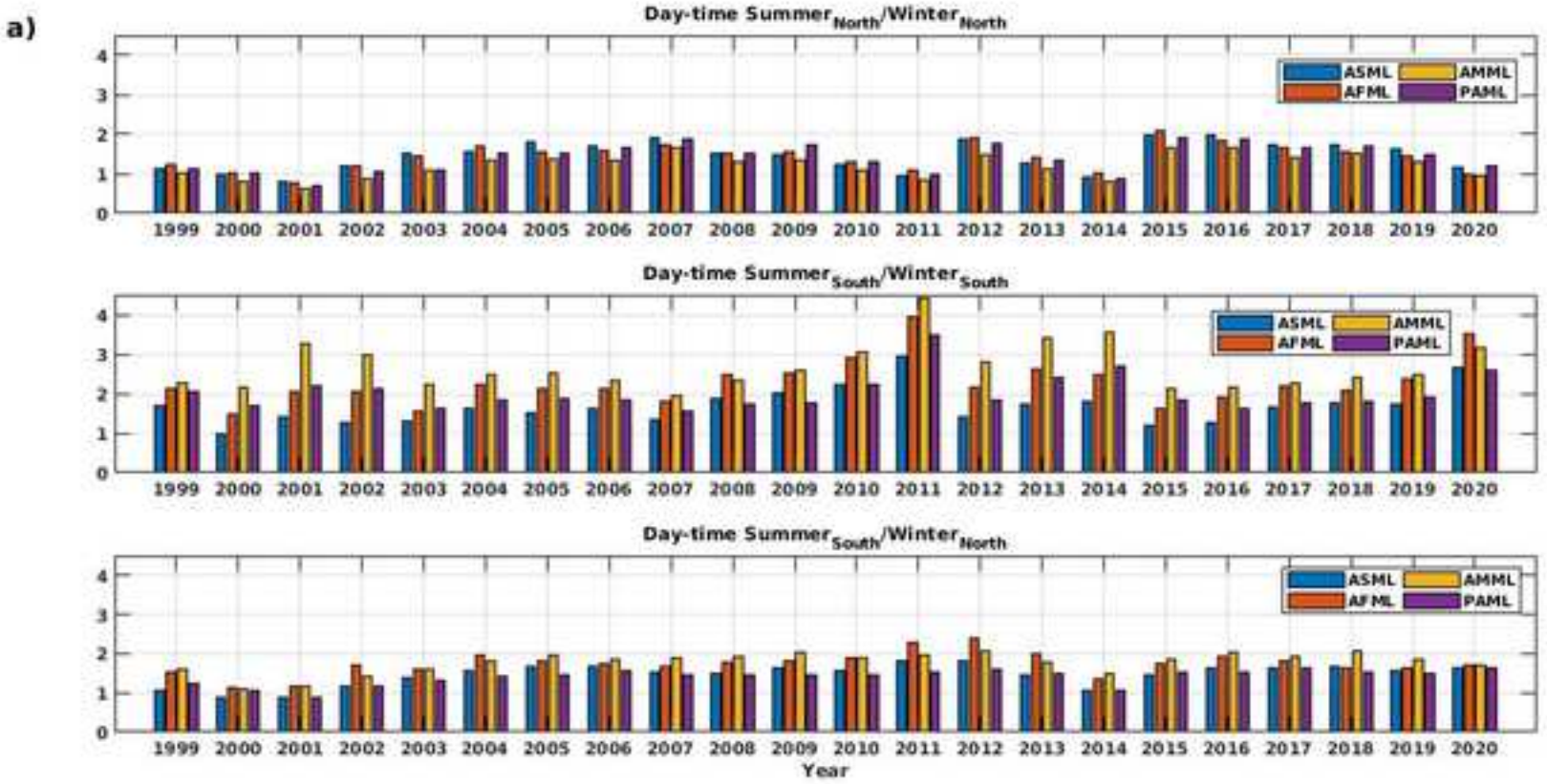

Figure 7a

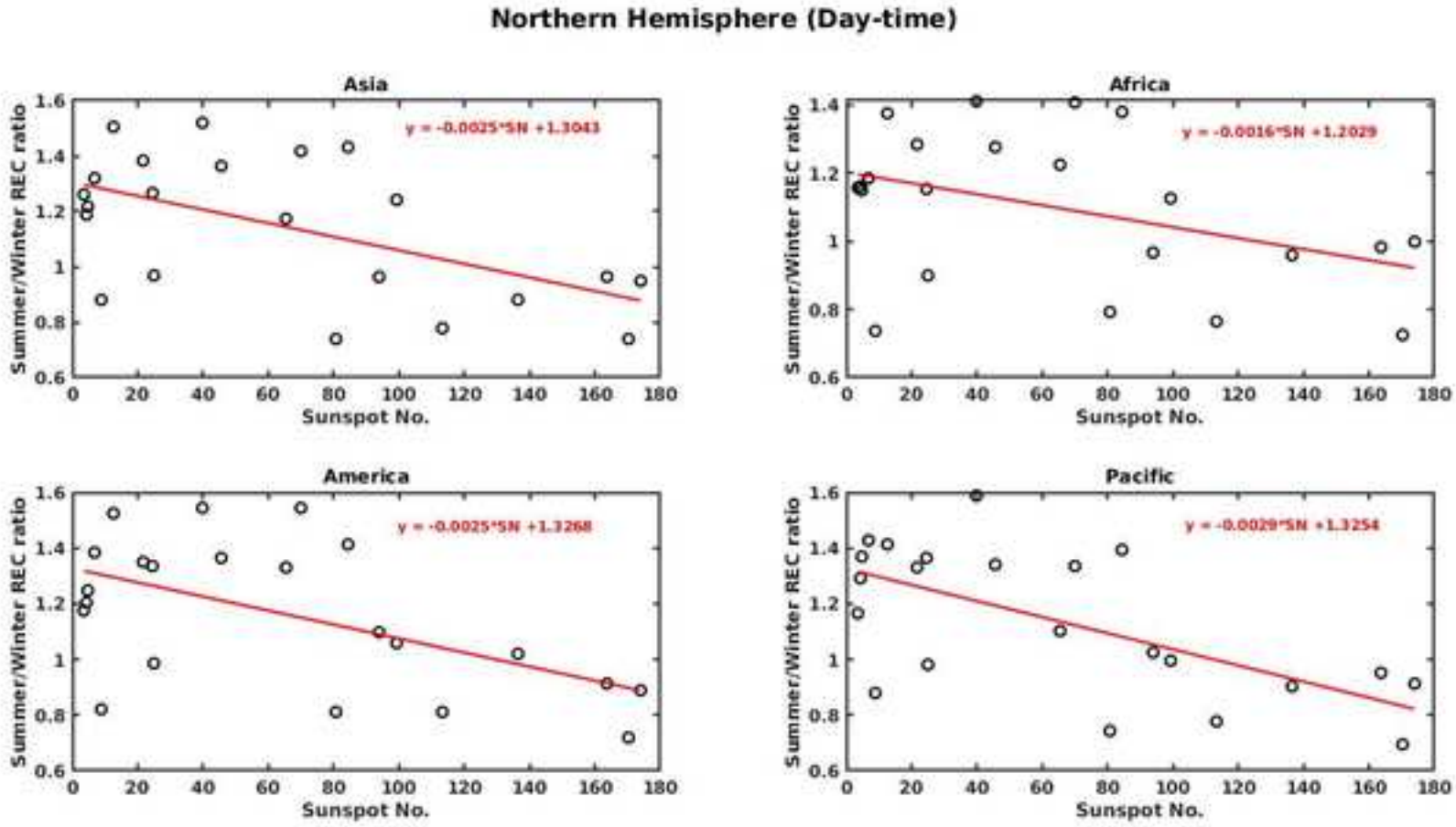

Figure 7b

Click here to access/download;Figure;Figure_7b.jpg

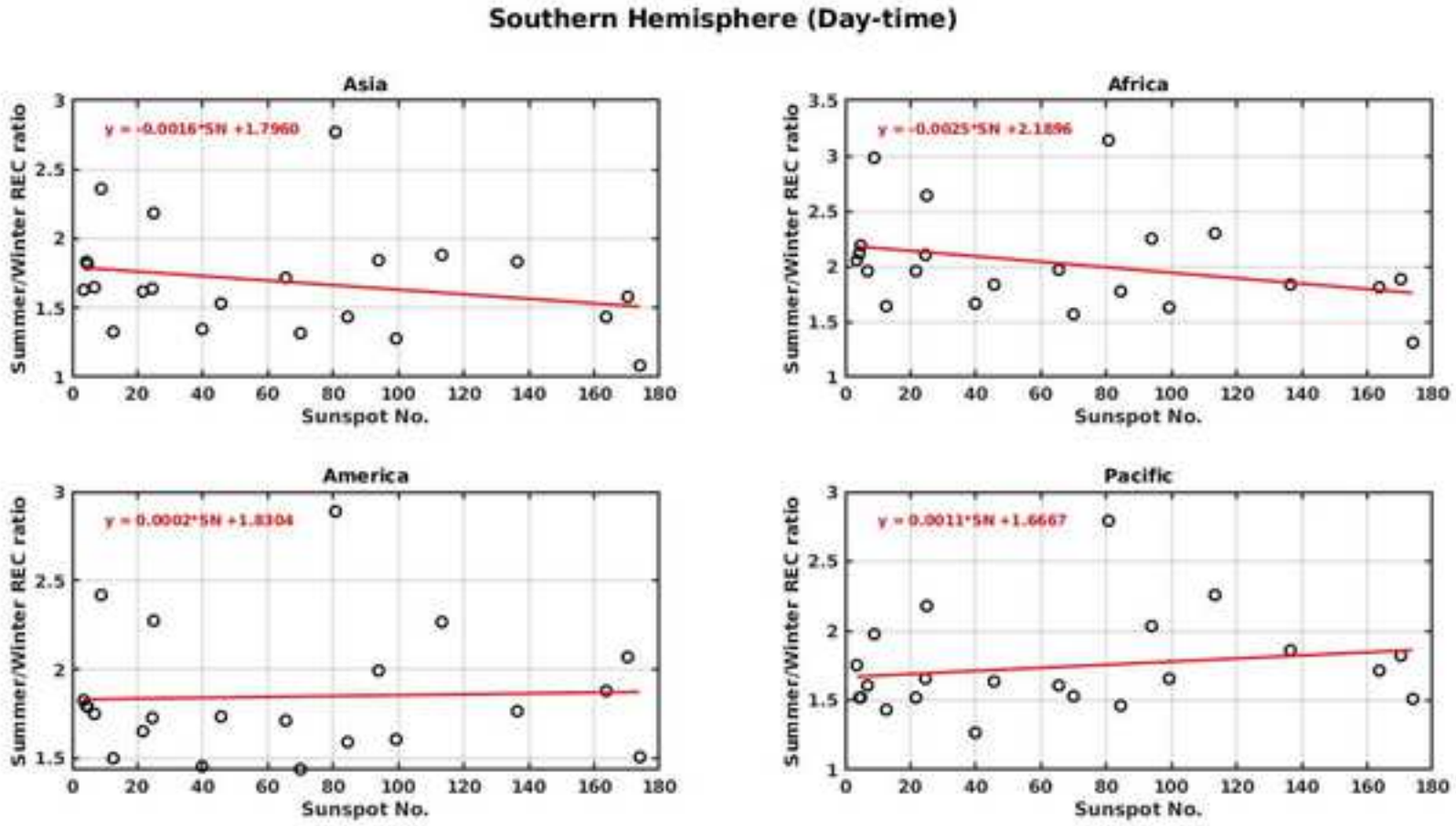

Figure 8a

Click here to access/download;Figure;Figure_8a.jpg

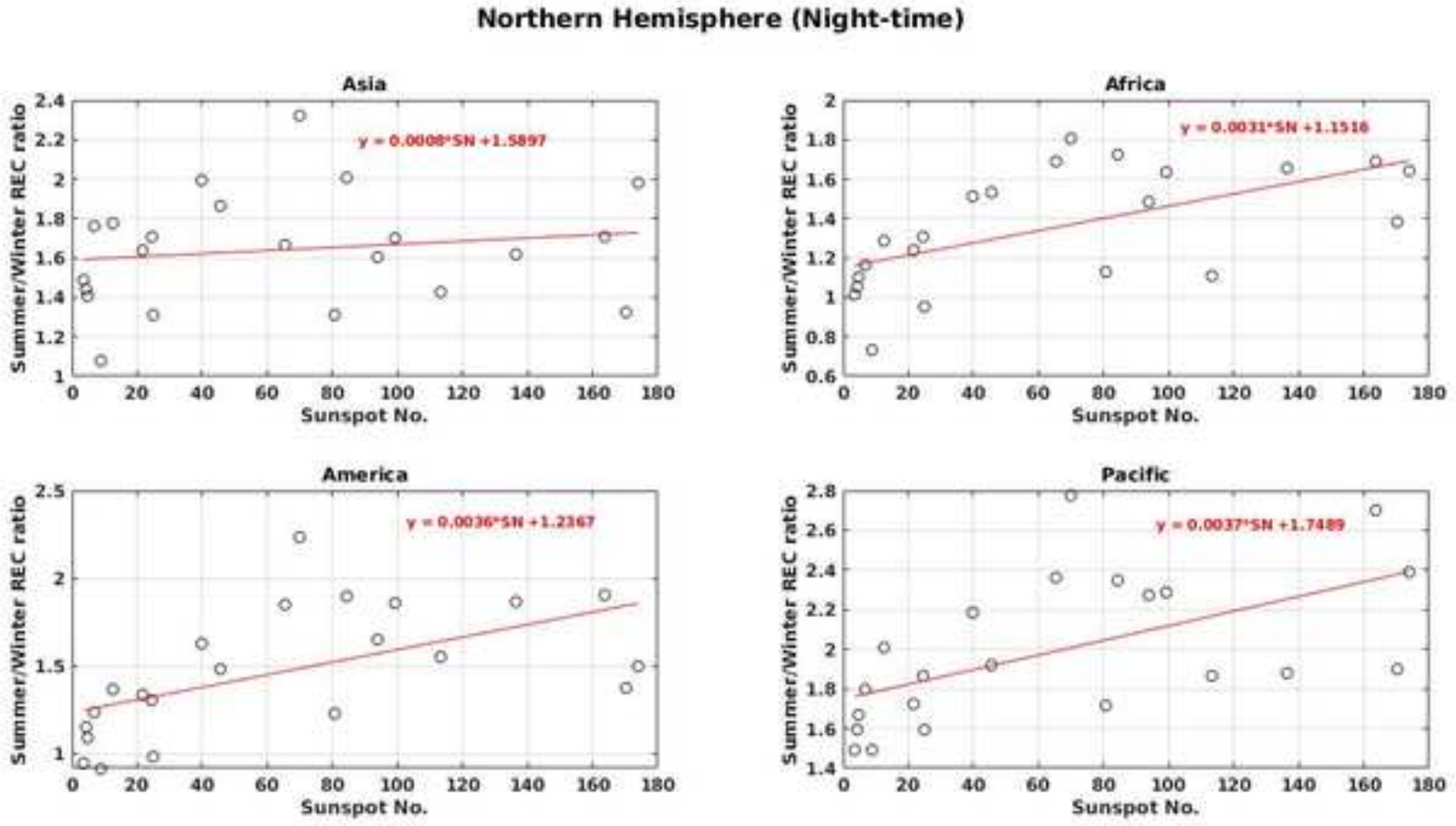

Figure 8b

Click here to access/download;Figure;Figure_8b.jpg

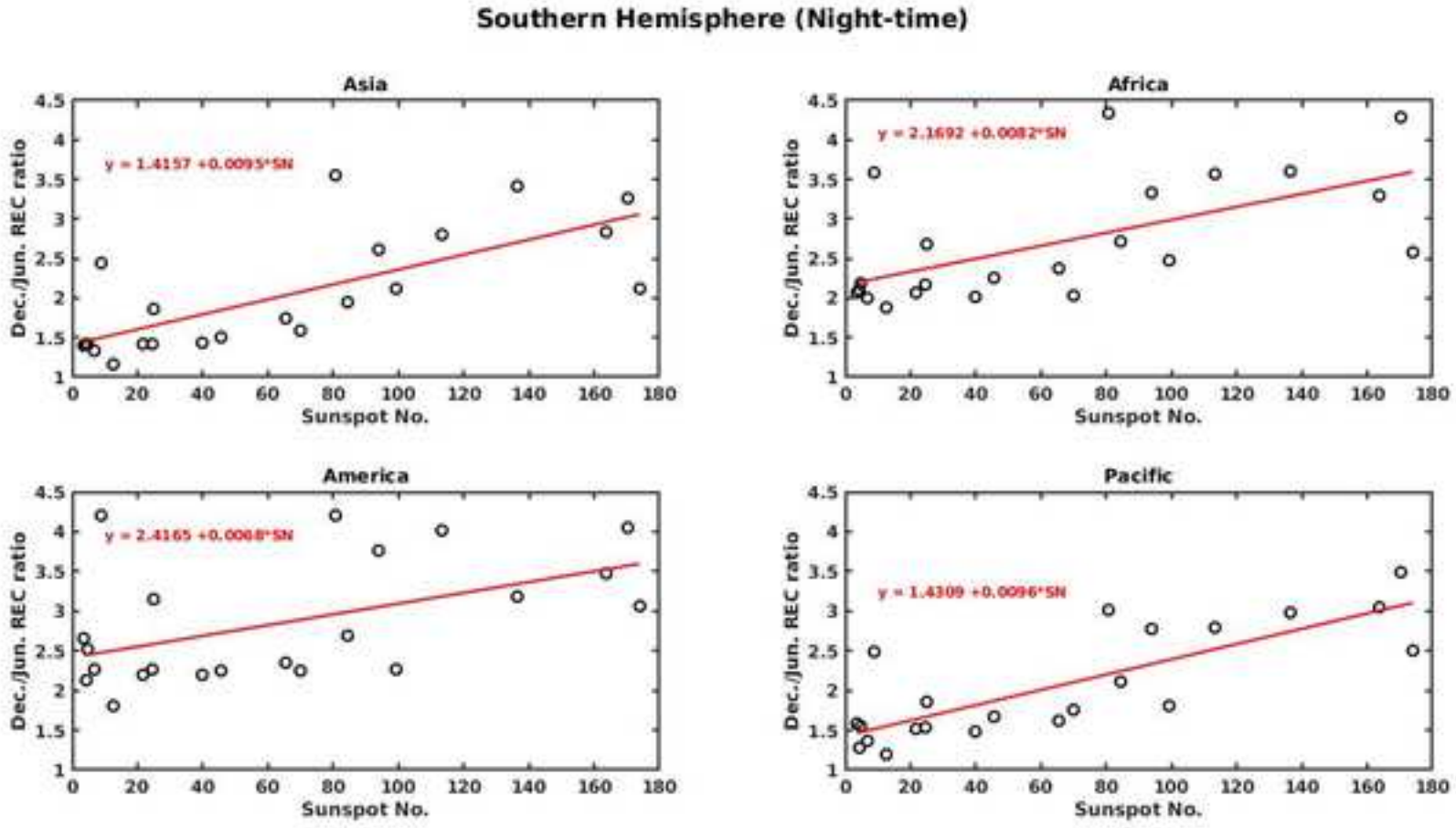

Figure 9a

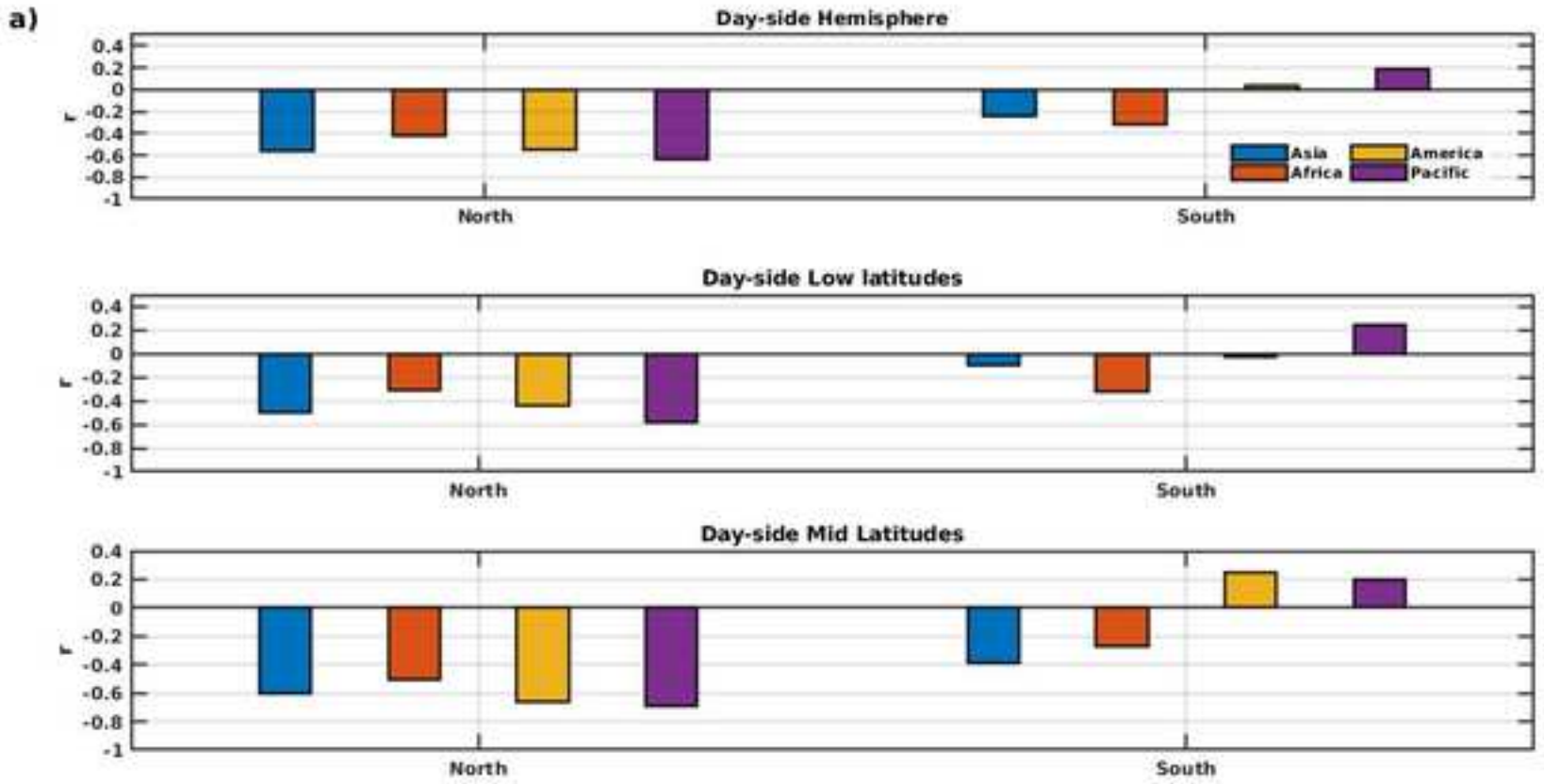

Figure 9b

Click here to access/download;Figure;Figure_9b.jpg

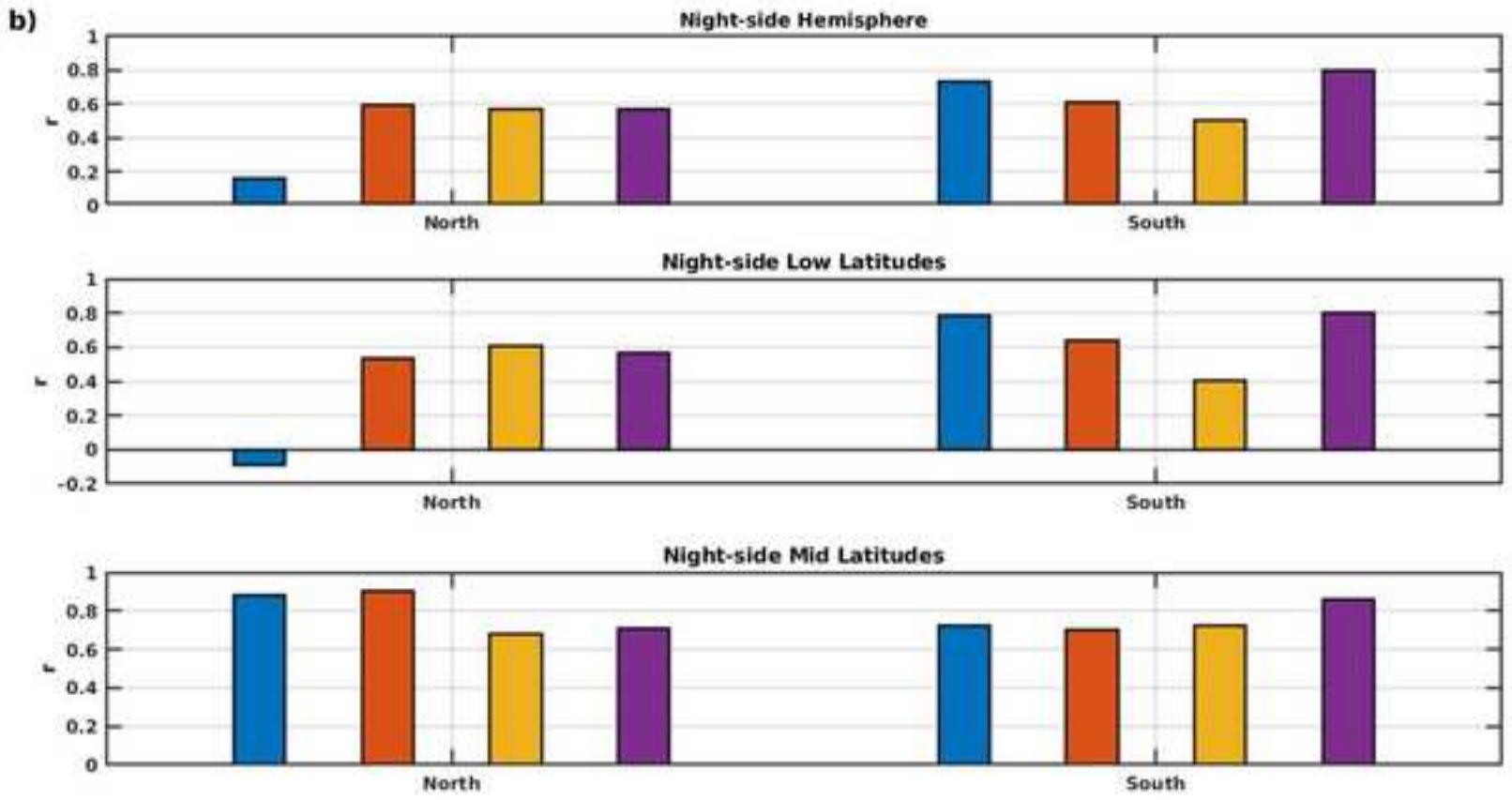

Figure 10a

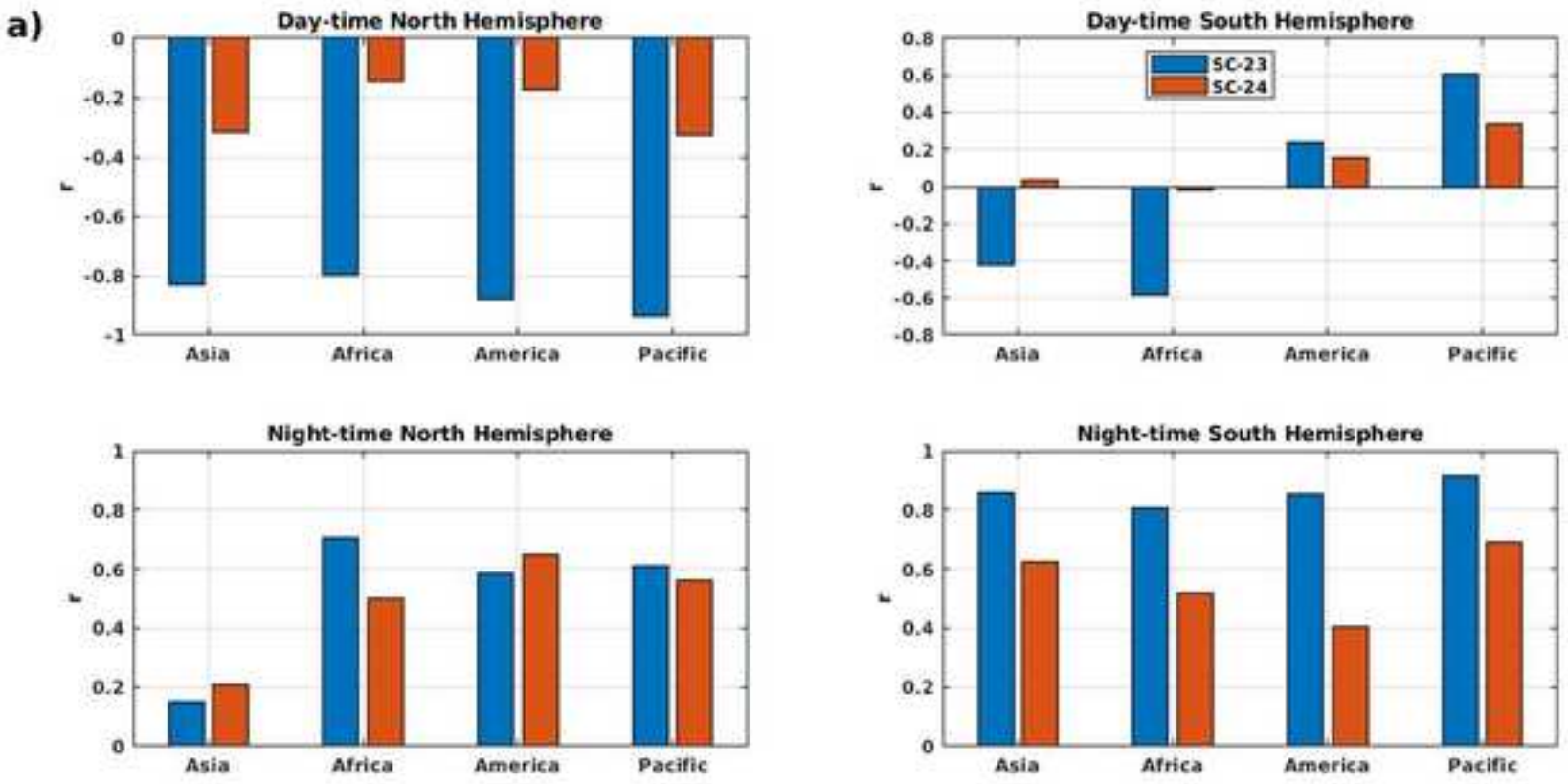

Figure 10b

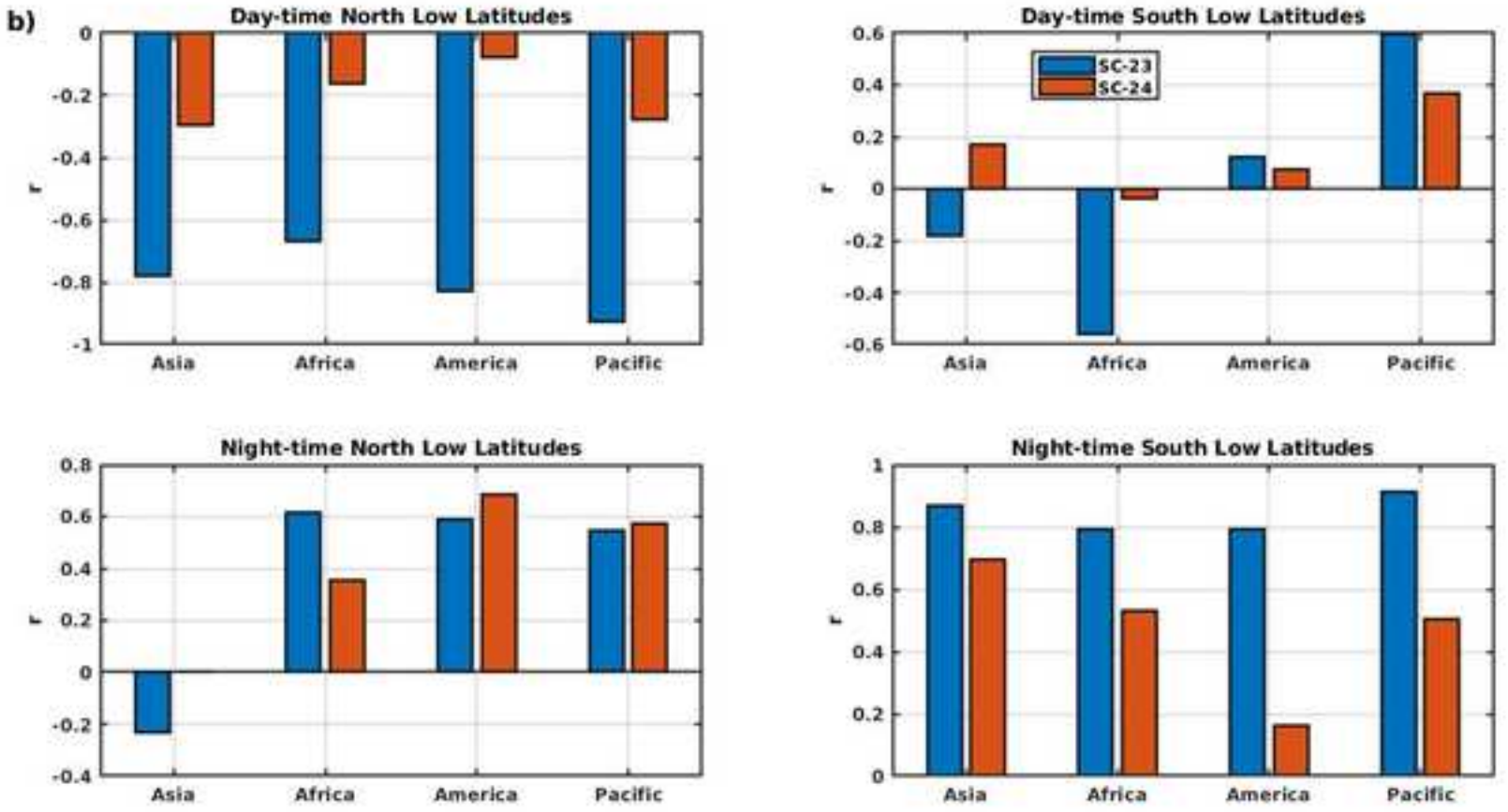

Figure 10c